Chemical Geology 386 (2014) 190–208

Contents lists available at ScienceDirect

Chemical Geology

journal homepage: www.elsevier.com/locate/chemgeo

Platinum-group element geochemistry of komatiite-derived 3.1 Ga ultramafic–mafic rocks and chromitites from the Nuggihalli greenstone belt, Western Dharwar craton (India)

Ria Mukherjee [a,*], Sisir K. Mondal [a], Hong Zhong [b], Zhong-Jie Bai [b], Vysetti Balaram [c], G.R. Ravindra Kumar [d]

[a] Department of Geological Sciences, Jadavpur University, Kolkata, India
[b] State Key Laboratory of Ore Deposit Geochemistry, Chinese Academy of Sciences, Guiyang, China
[c] National Geophysical Research Institute, Hyderabad, India
[d] Centre for Earth Science Studies, Trivandrum, India

ARTICLE INFO

Article history:
Received 10 July 2013
Received in revised form 28 July 2014
Accepted 6 August 2014
Available online 19 August 2014

Editor: L. Reisberg

Keywords:
Platinum-group elements (PGE)
Ultramafic–mafic rocks
Chromitites
Komatiites
Nuggihalli greenstone belt
Western Dharwar craton

ABSTRACT

The 3.1 Ga Nuggihalli greenstone belt in the Western Dharwar craton (southern India) comprises a sill-like layered ultramafic–mafic igneous complex with associated metasedimentary and metavolcanic (komatiitic to komatiitic basalt) schists that are enclosed by the tonalite–trondhjemite granodiorite suite of rocks (TTG). The sill-like layered complex is represented by a succession of chromitite-bearing serpentinite (after dunite) and peridotite, anorthosite, pyroxenite, and gabbro hosting magnetite bands. Extensive bulk-rock trace element and platinum-group element (PGE) geochemical study of the plutonic sill-like layered complex and the metavolcanic schists, suggest immobility of most trace elements (except La and Cu) and the PGEs, despite greenschist facies metamorphism and hydrothermal alteration experienced by the rocks. Their immobile nature is understood from good correlation of the trace elements and PGE with MgO and Cr. Other than chromitites and serpentinites all plutonic rocks show PPGE (Pd, Pt, Rh) enriched primitive-mantle normalized PGE patterns (Pd/Ir_N = 3.9–81.1) that are suggestive of fractionation of IPGEs (Ir, Os, Ru) by the early crystallizing chromite mineral, and the incompatible nature of PPGEs in the same. The chromitites show high PGE abundances ($\sum$PGE = 96–296 ppb), especially IPGEs ($\sum$IPGE = 63–223 ppb), due to the presence of inclusions of IPGE-bearing minerals. In the primitive-mantle normalized PGE plot the chromitites show an IPGE enriched pattern. The PPGE enriched pattern (Pd/Ir_N = 7.7–26) of the komatiitic to komatiitic basalt schists in a primitive-mantle normalized PGE plot indicates retention of IPGEs in the mantle or IPGE-bearing alloy saturation in the melt, while incompatible behavior of the PPGEs implies the sulfide undersaturated nature of the mantle source.

The PGE pattern of the metavolcanic schists resembles the pattern of early Archean (3.5 Ga) Barberton komatiites ($Pd/Ir_N^{Barberton}$ = 1–40.7; $Pd/Ir_N^{Nuggihalli}$ = 6.3–21.3), which corroborates our previous results based on REE study, and also resembles the pattern of komatiites from the 2.9 Ga Sandstone greenstone belt in the Youanmi Terrane of Western Australia ($Pd/Ir_N^{Sandstone}$ = 6). The metavolcanic schists exhibit the typical PGE depleted character observed in early Archean komatiites ($\sum PGE_{schist}$ = 0.4–27.2 ppb; $\sum PGE_{Barberton}$ = 15.0–20.8 ppb; $\sum PGE_{Youanmi\ Terrane,\ Western\ Australia}$ = 4.2–7.0 ppb) which is explained to be a result of progressive mixing of late veneer matter in the Earth's mantle with time. Pt fractionation in the Nuggihalli metavolcanic schists and in early or late Archean komatiites indicates Pt alloy dispersal in the lower mantle during crystallization of the primary magma ocean and a consequent formation of Pt-enriched and Pt-depleted isolated upper mantle domains that did not homogenize and mix away by 2.7 Ga.

In the plutonic layered sequence, pyroxenite represents a change from sulfide-undersaturation to sulfide-saturation. The pyroxenite represents a break in trend from the negative correlation of Pt and Pd with MgO displayed by the serpentinites and peridotites due to incompatible behavior of the PPGEs during lava differentiation, to the positive pattern displayed by the gabbro and metavolcanic schists due to attainment of sulfide saturation. Sulfide-saturation was probably triggered by fractional crystallization of olivine, chromite and pyroxenes. Chondrite-normalized REE patterns and a plot of incompatible elements negate the role of crustal contamination of the parental komatiitic magma. In addition, the absence of ambient sulfidic sediments rules out assimilation of crustal sulfur in the Nuggihalli rocks. The immiscible sulfides segregated from the Al-

* Corresponding author at: Department of Geological Sciences, Jadavpur University, 188 Raja S.C. Mullik Road, Kolkata-700032, India. Tel.: +91 33 24572730.
E-mail address: ria.mkrj@gmail.com (R. Mukherjee).

http://dx.doi.org/10.1016/j.chemgeo.2014.08.007

depleted komatiitic parental magma concentrating the PGEs during crystallization of the pyroxenes that accumulated to form pyroxenite.

1. Introduction

The platinum-group elements (PGEs: Os, Ir, Ru, Rh, Pt and Pd) have been used as geochemical tracers to study the different igneous processes operating in the Earth like magmatic fractionation, mantle melting and melt–rock interactions, and also to understand the nature and evolution of the source mantle (e.g., Maier et al., 2009; Puchtel et al., 2009, 2014; Lorand et al., 2013). Their chalcophile nature makes them useful for studying the sulfide-saturation history of the melt (e.g., Hamlyn and Keays, 1986), thus PGEs are effective tools in lithogeochemical exploration for Ni–Cu-sulfide deposits (e.g., Fiorentini et al., 2010). In the present study we have utilized whole-rock PGE geochemistry of sill-like chromitite- and magnetite-bearing ultramafic–mafic rocks and metavolcanic (komatiitic to komatiitic basalt) schists from the Archean Nuggihalli greenstone belt (3.1 Ga; Mukherjee et al., 2012) to understand the sulfide-saturation history of the parental melt. The sill-like ultramafic–mafic rocks and associated metavolcanics in Archean greenstone belts are genetically related to high-Mg magmas like komatiites, high-Mg siliceous magmas or boninites (e.g., Rollinson, 1997; Mondal et al., 2006; Prendergast, 2008; Mukherjee et al., 2012). Geochemical study of the platinum-group of elements in high-Mg magmas like komatiites is essential to understand the PGE character of the mantle source, as komatiites are high-degree partial melts and sulfide-undersaturated (Maier et al., 2003; Puchtel et al., 2009, 2014). In addition, study of PGEs in Archean high-Mg magma derived rocks is critical to understand the evolution of the Archean mantle.

In the Archean, PGE mineralization is associated with both major chromite and Ni–Cu-sulfide deposits that occur within the greenstone belts (e.g., Lesher and Keays, 2002). Common examples of PGE mineralization associated with chromite deposits include the Jamestown igneous complex (Barberton greenstone belt, South Africa; DeWit and Tredoux, 1987), the Nuasahi ultramafic–mafic complex (Singhbhum craton, eastern India; Mondal and Zhou, 2010), the Bird River sill (Bird River greenstone belt; Peck et al., 2002) and the Lac des Iles intrusive complex in the Superior craton, Canada (Wabigoon sub-province; Hinchey et al., 2005). Those associated with Ni–Cu-sulfide deposits are more common in the volcanic rocks of the greenstone belt e.g., komatiites from the Abitibi greenstone belt (Superior craton, Canada; Puchtel et al., 2004), the Agnew-Wiluna greenstone belt and the Kalgoorlie Terrane (Yilgarn craton, Western Australia; Keays et al., 1981; Fiorentini et al., 2007, 2012; Barnes et al., 2012, 2013).

In India, significant PGE mineralization ($PGE_{total} \approx$ 258–24,100 ppb) has solely been reported from the Nuasahi ultramafic–mafic complex (Mondal and Baidya, 1997; Mondal and Zhou, 2010), where the mineralized zone is located within a shear zone masked by the breccia that separates a lower chromiferous ultramafic unit from an upper gabbro unit.

Detailed PGE geochemical study has not been conducted so far in the Nuggihalli greenstone belt. Our present work therefore focuses on detailed geochemical study of platinum-group elements of the plutonic ultramafic–mafic igneous complex, and the associated metavolcanic schist rocks in the Nuggihalli greenstone belt. We have addressed the whole-rock major and trace element study of these rocks in our previous work (Mukherjee et al., 2012) to understand about the nature of the parental melt and magmatic fractional crystallization history of the rocks in the greenstone belt. In this study a larger number of samples has been analyzed for major and trace elements to augment our earlier findings.

2. Geological background

The Dharwar craton is divided into an eastern and western component by a 500 km long body of Closepet granite (Fig. 1A). The Western Dharwar craton consists of both early Archean (3.4–3.1 Ga; Table 1) and meso- to late Archean greenstone belts (3.0–2.6 Ga; Table 1; Mukherjee et al., 2012 and references therein). The rocks of the early Archean greenstone belts are also known as the Sargur Group (Swami Nath and Ramakrishnan, 1981). The Sargur Group is comprised of conformable units of volcano-sedimentary rocks and sill-like plutonic ultramafic–mafic rocks, all of which are encompassed by the tonalite–trondhjemite-granodiorite suite (TTG; Fig. 1A). The Sargur Group of rocks are deformed and metamorphosed to the low-grade greenschist facies, despite which primary igneous textures are preserved and the protoliths can still be identified. The volcanic rocks are mainly komatiites, komatiitic basalts and tholeiites (Ramakrishnan 2009), which are now represented by tremolite–actinolite–chlorite–hornblende–quartz bearing schists. The metasedimentary rocks are fuchsite-quartzites, banded-iron formations, bedded barites, and kyanite–garnet-bearing quartzites and mica schists (Ramakrishnan, 1981).

The sill-like chromitite-bearing layered ultramafic–mafic rocks are the focus of our study. They occur in the early Archean greenstone belts (Sargur Group) of Nuggihalli–Holenarsipur–Krishnarajpet–Nagamangala in the Western Dharwar craton. The sill-like rocks occur as *en echelon*, lenticular fragments (length ≈ 30–60 km; width ≈ 2–6 km) that occupy nearly a 250 km long N–S zone in the craton (Nijagunappa and Naganna, 1983). The Sargur Group of rocks is stratigraphically followed by the rocks of the meso-to late Archean greenstone belts, known as the Dharwar Supergroup (Fig. 1A), following an unconformity. The TTG suite acts as the basement for the Dharwar Supergroup, which are later intruded by a N–S trending conspicuous body of alkali feldspar-rich granite known as the Closepet granite (2.5 Ga; Taylor et al., 1988). The general stratigraphy of rocks in the Western Dharwar craton is tabulated in Table 1.

The Nuggihalli greenstone belt (length 60 km; width 2 km), which is the area of our study, occurs within the Western Dharwar craton as a linear belt with a NNW–SSE disposition (Fig. 1B). The sill-like ultramafic bodies host chromite deposits whereas the mafic sequence contains magnetite bands, which are all encompassed within the TTG suite. The plutonic ultramafic–mafic rocks and the metavolcanic schists are well exposed in the Tagdur mining district of the Nuggihalli greenstone belt (Fig. 1B). The stratigraphic column of all the rocks exposed in the greenstone belt has been illustrated in Fig. 2. A detailed description of the ultramafic–mafic unit, including the chromitite bodies, is provided in Mukherjee et al. (2010) and Mukherjee et al. (2012). We have recently dated the sill-like plutonic ultramafic–mafic rocks in the greenstone belt at 3150 ± 120 Ma by the whole-rock Sm–Nd isochron method (Mukherjee et al., 2012). The age is found to be similar (within the error limits) to the reported ages of komatiites in the craton.

The rocks in the greenstone belt are metamorphosed (greenschist facies) and rarely primary minerals are preserved. The igneous protolith of the ultramafic–mafic cumulate rocks was inferred from their present altered and metamorphosed mineralogy. The serpentinites represented an altered dunite body, while the presence of metamorphic minerals like chlorite, tremolite, actinolite and talc in the cumulate rocks implied the protolith to be a peridotite and pyroxenite (depending on the modal proportions of the minerals). The anorthosite and gabbro were easy to identify due to predominance of cumulus plagioclase in the former and occurrence of cumulus plagioclase with interstitial chlorite and

actinolite in the latter. The detailed petrographic descriptions of the ultramafic–mafic cumulate rocks are tabulated in Table 3. The ultramafic–mafic rocks in the Nuggihalli greenstone belt are deformed by multiple phases of superposed folding, because of which they appear as dismembered and lenticular bodies. Despite this, the sill-like ultramafic–mafic rocks preserve primary igneous textures as a result metamorphic nomenclatures will not be used for them in the following sections.

The chromitite ore-bodies hosted within the serpentinite and peridotite range in length from 50 to 500 m with a width of 15 m (Fig. 2). The ore-bodies exhibit different shapes (e.g., banded, layered, pod-shaped, lenticular, and sigmoidal; Fig. 3) owing to superposed folding common in the greenstone belt (Mukherjee et al., 2010). The ore-bodies have predominantly N–S and NW–SE disposition with dip of 75–80° towards the east. The strike of the ore-body varies and is sometimes E–W with dip towards the north (Fig. 3D). The anorthosite layer is not consistently exposed in all outcrops. It had been reported in the Byrapur chromite mine in association with serpentinite and pyroxenite (Radhakrishna and Vaidyanadhan, 1994), and also occurs in the Jambur mine as a lens-shaped E–W trending unit (width ≈ 130 m) interlayered with serpentinite. The lower band of titaniferous–vanadiferous magnetite hosted within gabbro (Fig. 2) shows disseminated sulfide mineralization of chalcopyrite and pyrite with minor pentlandite, pyrrhotite and cubanite (Radhakrishna et al., 1973; Pandit, 1975; Mukherjee et al., 2013).

The metavolcanic komatiitic to komatiitic basalt schists (Fig. 2) show grain size variations, have stronger penetrative deformation fabrics, and exhibit lens-shaped geometry that conforms to the general appearance of the sill-like ultramafic–mafic unit.

Samples for this study cover all the different lithological units (except TTG), and are collected from the mine sections and outcrops in the Tagdur, Byrapur and Jambur mines of the Nuggihalli greenstone belt (Fig. 1B). Table 2 (available online) lists details of samples used in this study, and the petrographic descriptions are tabulated in Table 3. In addition, some of the samples already studied by Mukherjee et al. (2012) for isotope, major and trace element geochemistry are used in this present study for PGE. The readers are referred to Mukherjee et al. (2012) for details of those samples.

3. Analytical methods

The analytical methodology for major elements has been described in detail in Mukherjee et al. 2012 and summarized here. Major elements for the samples were analyzed at the Centre for Earth Science Studies (Trivandrum, India), using a Bruker S4 Pioneer Wavelength Dispersive X-ray Fluorescence (WD-XRF) spectrometer. Fused glass discs (30 mm) used for analysis were prepared by fusing exactly 1 g of finely powdered sample mixed with 5 g of lithium tetra-metaborate flux in a platinum crucible at 1100 °C using Claisse Fluxer, following determination of loss on ignition of the samples. The standards used were ultramafic rock standards from the USGS, DTS1 and DTS2 and UB-N from CRPG (France). Duplicate analyses of the standards and the certified values are enlisted in Table 4a (available online). The detection limit for major elements was ~0.01% and analytical precision is better than 1%. The major element oxides have been recalculated on an anhydrous basis and tabulated in Table 4c. Totals of major element oxides are 100 ± 1 wt.%. Trace element concentrations on bulk solutions were analyzed by ICP-MS on the Perkin Elmer Sciex Elan DRC II facility of the National Geophysical Research Institute (Hyderabad, India). Closed-beaker digestion of 0.05 g samples were conducted using 10 ml acid mixture of HF–HNO_3–HCl in the ratio 7:3:2 (Roy et al., 2007). The standards used were UB-N for the ultramafic rocks, JGb-1 for the mafic rocks and FeR-4 for magnetite. The duplicate analyses and certified value of the standards are tabulated in Table 4b (available online), while trace element values of the samples from our study are enlisted in Table 4c. The trace and REE data obtained for the standards and the rock samples under investigation were found to be in good agreement with the certified data. The precisions achieved were <5% RSD with comparable levels of accuracy in most cases (Roy et al., 2007).

The PGEs were analyzed by the Ni–S fire assay procedure at the National Geophysical Research Institute (NGRI) and by the Carius tube technique at the State Key Laboratory of Ore Deposit Geochemistry (SKLODG), Institute of Geochemistry, Chinese Academy of Sciences (Guiyang, China). The PGEs were analyzed by ICP-MS following a Ni–S fire assay preconcentration of a 10 g sample using intermediate flux of borax (80 g), sodium carbonate (40 g), sulfur powder (1.2 g), nickel powder (2 g), silica (6 g), and calcium fluoride (1.5 g) in a muffle furnace at 1050 °C for 1 h 20 min (Balaram et al., 2006; Roy et al., 2010). The fire assay procedure was followed by dissolution of the sulfide beads in concentrated HCl followed by Te precipitation of PGE and treatment of the precipitate by aqua regia (Balaram et al., 2006; Roy et al., 2010). The standards used were WMG-1 for the ultramafic rocks and WGB-1 for the mafic rocks. The results of the replicate analyses along with certified values from the NGRI lab are given in Table 5a (available online). The precisions obtained were found to be better than 8% RSD in general for all PGE with comparable accuracies (Chalapathi Rao et al., 2014). There is also a good agreement between the certified values for PGE and the values obtained in this study for WMG-1 (Table 5a). The detection limits were in the range of 0.04-0.16 ng while the procedural blanks for different PGE obtained varied from below detection to 0.003 ng (Chalapathi Rao et al., 2014).

Platinum-group elements were determined by isotope dilution (ID)-ICP-MS using an improved Carius tube technique from the State Key Laboratory of Ore Deposit Geochemistry (SKLODG), Institute of Geochemistry, Chinese Academy of Sciences (Guiyang, China). The mono-isotope element Rh was measured by external calibration using a ^{194}Pt spike as internal standard (Qi et al., 2004). Eight grams of rock powder and an appropriate amount of enriched isotope spike solution containing ^{193}Ir, ^{101}Ru, ^{194}Pt, and ^{105}Pd were digested using ~27 ml aqua regia in a 75 ml Carius tube placed in a sealed, custom-made, high pressure, water-filled autoclave (Qi et al., 2007). 20 ml HF was then added to the transferred solution to decompose the remaining silicate minerals. After centrifuging, the solution was used to preconcentrate PGE by Te-coprecipitation, as described in Qi et al. (2004). Cu, Ni, Zr and Hf were removed passing through a mixed ion exchange column which contains a Dowex 50 WX 8 cation exchange resin and a P507 extraction chromatograph resin to minimize their interference. The total procedural blanks were lower than 0.003 ng for Ir and Ru; 0.002 ng for Rh and Pt; and 0.013 ng for Pd. The results of the standard reference material WGB-1 (gabbro) agree well with the values reported by Qi et al. (2008) (Table 5a, available online). The accuracies are estimated to be better than 10% for all PGEs. PGE data of the samples in this study are tabulated in Table 5c.

4. Geochemical variations

4.1. Major and trace elements

In a previous work Mukherjee et al. (2012) studied the major element, trace element and isotope geochemistry of selected ultramafic–mafic

Fig. 1. (A) Geology of the Dharwar craton showing location of the Nuggihalli greenstone belt (after Murthy, 1987; cited in Devaraju et al., 2009). Inset map illustrates the geology of the Indian shield showing location of the Dharwar craton (compiled by Mondal et al., 2006; after Leelananadam et al., 2006; Radhakrishna and Naqvi, 1986). (B) Geology of the Nuggihalli greenstone belt (after Jafri et al., 1983; cited in Devaraju et al., 2009) is shown at the left-hand corner. The dotted boundary denotes the area in the map that has been enlarged (right-hand side) to show the chromite mining districts and sample locations of this study.

A

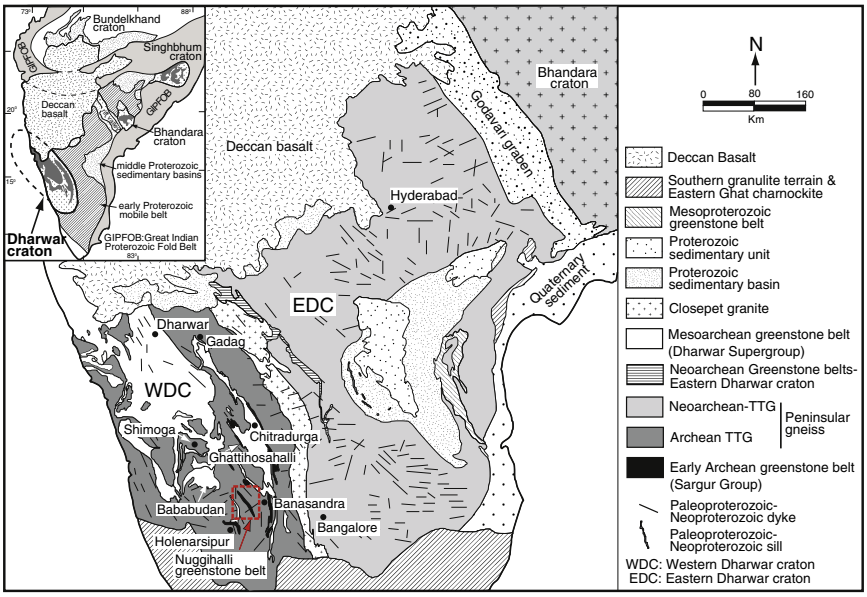
Bundelkhand craton
Singhbhum craton
Deccan basalt
Bhandara craton
middle Proterozoic sedimentary basins
early Proterozoic mobile belt
GIPFOB:Great Indian Proterozoic Fold Belt
Dharwar craton
Deccan basalt
Bhandara craton
Godavari graben
Hyderabad
EDC
Quaternary sediment
Dharwar
Gadag
WDC
Shimoga
Chitradurga
Ghattihosahalli
Bababudan
Banasandra
Bangalore
Holenarsipur
Nuggihalli greenstone belt
N
0 80 160
Km
Deccan Basalt
Southern granulite terrain & Eastern Ghat charnockite
Mesoproterozoic greenstone belt
Proterozoic sedimentary unit
Proterozoic sedimentary basin
Closepet granite
Mesoarchean greenstone belt (Dharwar Supergroup)
Neoarchean Greenstone belts-Eastern Dharwar craton
Neoarchean-TTG
Archean TTG
Peninsular gneiss
Early Archean greenstone belt (Sargur Group)
Paleoproterozoic-Neoproterozoic dyke
Paleoproterozoic-Neoproterozoic sill
WDC: Western Dharwar craton
EDC: Eastern Dharwar craton

B

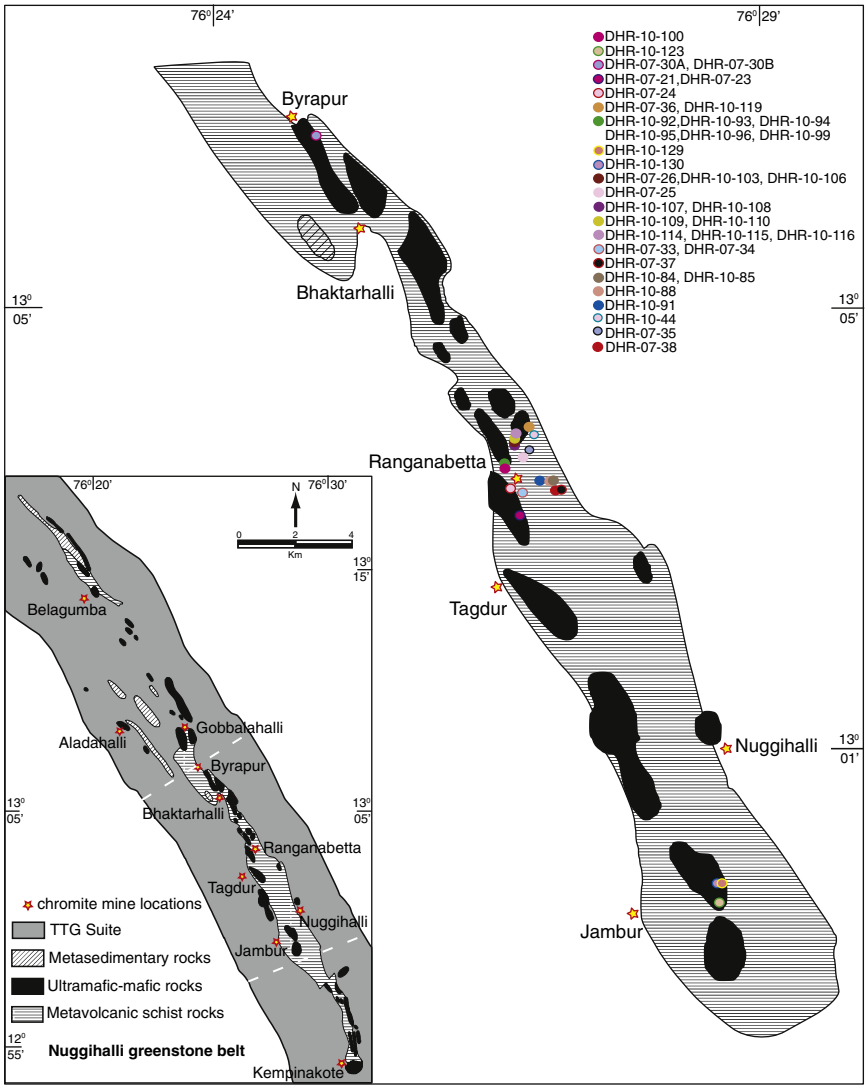
76°24'
76°29'
13°05'
Byrapur
Bhaktarhalli
Ranganabetta
Tagdur
Nuggihalli
13°01'
Jambur
DHR-10-100
DHR-10-123
DHR-07-30A, DHR-07-30B
DHR-07-21,DHR-07-23
DHR-07-24
DHR-07-36, DHR-10-119
DHR-10-92,DHR-10-93, DHR-10-94
DHR-10-95,DHR-10-96, DHR-10-99
DHR-10-129
DHR-10-130
DHR-07-26,DHR-10-103, DHR-10-106
DHR-07-25
DHR-10-107, DHR-10-108
DHR-10-109, DHR-10-110
DHR-10-114, DHR-10-115, DHR-10-116
DHR-07-33, DHR-07-34
DHR-07-37
DHR-10-84, DHR-10-85
DHR-10-88
DHR-10-91
DHR-10-44
DHR-07-35
DHR-07-38
76°20'
N
76°30'
0 2 4
Km
13°15'
Belagumba
Gobbalahalli
Aladahalli
Byrapur
Bhaktarhalli
Ranganabetta
Tagdur
Nuggihalli
Jambur
chromite mine locations
TTG Suite
Metasedimentary rocks
Ultramafic-mafic rocks
Metavolcanic schist rocks
12°55'
Nuggihalli greenstone belt
Kempinakote

Table 1
Stratigraphy and crustal evolution of the Western Dharwar craton (Mukherjee et al., 2012 and references therein).

	Stratigraphic unit	Age
Younger granites	Closepet–Chitradurga–Arsikere granites	2.5–2.4 Ga
Late Archean greenstone sequence	Bababudan–Chitradurga–Shimoga greenstone sequences containing metavolcanics and metasediments	3.0–2.6 Ga
	Cumulate ultramafic–mafic suite hosting nickel sulfide and PGE mineralization, chromite and magnetite deposits within Bababudan and Shimoga greenstone belt	2.9–2.8 Ga
Early Archean - Mesoarchean greenstone sequence with TTG	TTG (Peninsular Gneiss)	3.4–2.9 Ga
	Sargur Group metavolcanics and metasediments including sill-like layered ultramafic–mafic plutonic suite containing chromite and magnetite deposits	3.4–3.0 Ga

rocks from the Nuggihalli greenstone belt. The variation in MgO content of the metavolcanic schists indicated that some were komatiitic in composition (e.g., 28 wt.% MgO of DHR-07-37, 33 wt.% MgO of DHR-10-84) while the rest were komatiitic basalts (Table 4c; Mukherjee et al., 2012). The authors compared the plutonic ultramafic–mafic and surrounding metavolcanic schist rocks with typical Al-depleted and undepleted komatiite and komatiitic basalt, and komatiite from the early Archean greenstone belts (e.g., J.C. Pura greenstone belt; Jayananda et al., 2008) of the Western Dharwar craton. In this study a larger number of samples have been included to augment our earlier findings by combining magmaphile major, trace and platinum-group element data. The major elements show a negative relation with MgO despite some scattering due to alteration (Fig. 5A–F). The trace elements Ni and Cr show positive variations with MgO (Fig. 5G, H), while Cu, La, Nd and Gd display negative relations (Fig. 5I–L) that reflect the incompatible nature of these elements. The scattered Cu distribution in the ultramafic–

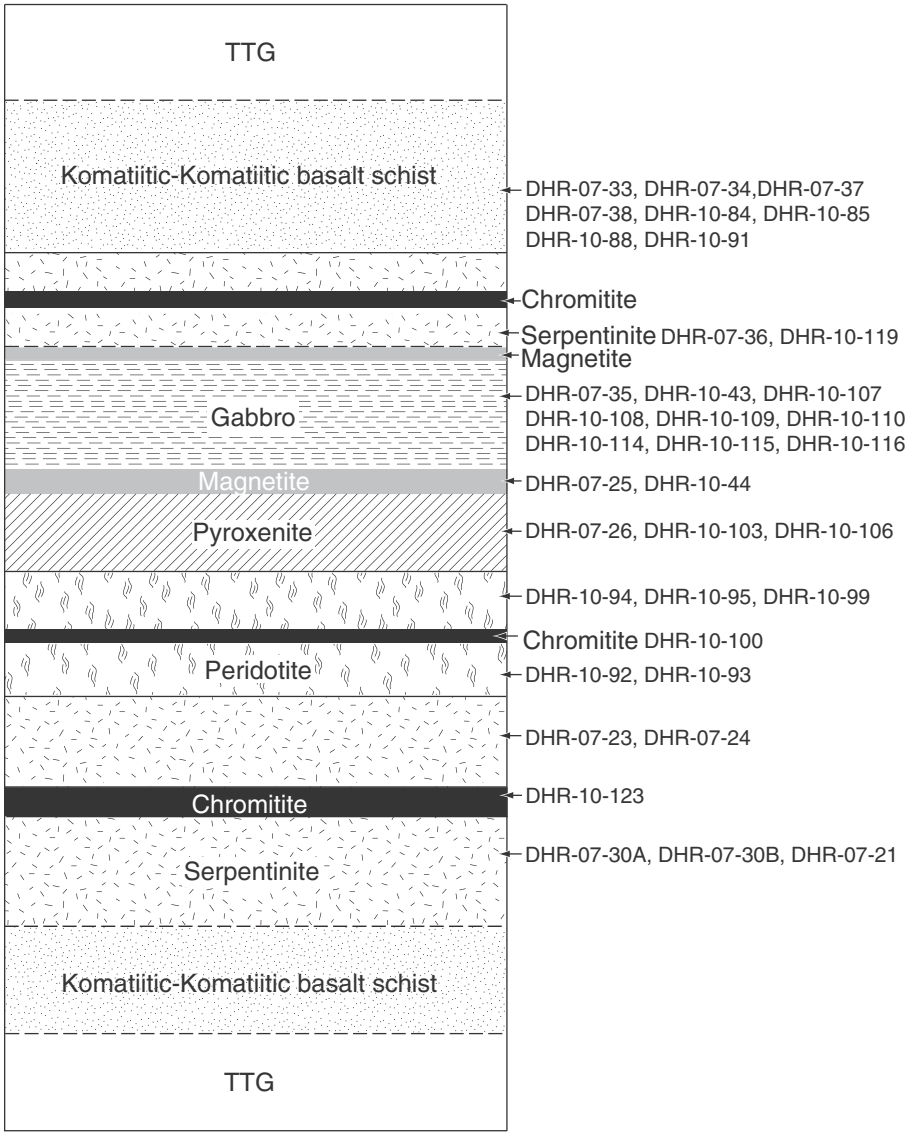

Fig. 2. Lithostratigraphy of the sill-like ultramafic–mafic plutonic rocks and the surrounding metavolcanic schists in the Nuggihalli greenstone belt. Samples collected from each lithounit have been indicated with detailed descriptions in Table 2. The anorthosite has been excluded from the stratigraphic column as its exposure is poor and its occurrence is limited to only certain chromite mining districts like Jambur.

Table 3
Petrographic description of ultramafic–mafic plutonic and metavolcanic rocks from the Nuggihalli greenstone belt.

Lithology	Number of samples analyzed in present study	Petrography
Serpentinite	7 (PGE) 1 (trace) 1(major)	Antigorite, chlorite, magnesite, accessory chromites. Magnesite proportion high (≈25–35% modal) in upper serpentinite (DHR-07-36, DHR-10-119). Serpentine minerals exhibit interpenetrating, mesh and pseudomorph textures.
Chromitite	2 (PGE) 2 (trace)	Coarse-medium grained, euhedral, polygonal chromite with intercumulus magnesite, antigorite and chlorite. Massive, spot, schlieren-bands and net-texture common (Fig. 4A). Disseminated sulfides (millerite with minor niccolite; 20–50 μm; Fig. 4B) in interstitial spaces, and inclusions (0.5–1.0 μm) along with rare platinum-group of minerals (laurite).
Peridotite	6 (PGE) 3 (trace) 3 (major)	Actinolite, chlorite, tremolite, talc, accessory chromite. Rock fine-grained, schistose.
Anorthosite	2 (PGE)	Coarse cumulus plagioclase surrounded by intercumulus actinolite, chlorite and minor oxide grains.
Pyroxenite	3 (PGE) 2 (trace) 2 (major)	Actinolite, remnant hypersthene, chlorite, quartz, ilmenite. Subhedral sulfide inclusions (2–15 μm) (mss) occur individually or in multiples (Fig. 4D).
Magnetite	1 (PGE)	Rock coarse-grained. Magnetite extensively oxidized to hematite with ilmenite exsolution along crystallographic planes or as blebs (Fig. 4E). Remnant magnetite rarely preserved. Grains are sintered and interstitial chlorite grains sheared. Coarse-medium, subhedral chalcopyrite and pyrite occur within oxide grains, oxide-chlorite and oxide-oxide contacts (Fig. 4E).
Gabbro	9 (PGE) 5 (trace) 5 (major)	Coarse-grained with cumulus texture. Plagioclase, chlorite, actinolite, quartz, coarse accessory magnetite (Fig. 4F), and ilmenite. Minor sulfide disseminations present.
Schists	8 (PGE) 4 (trace) 4 (major)	Komatiitic schists (sample DHR-07-37, DHR-10-84)—actinolite, chlorite, minor plagioclase (altered to epidote), anhedral hematite, lath-shaped ilmenite (occur at grain boundaries of silicate minerals) and talc. Crenulations, puckers, chevron folds common in sample DHR-07-37. Komatiitic basalt schists (sample DHR-07-33, DHR-07-34, DHR-07-38, DHR-10-85, DHR-10-88, DHR-10-91)—coarse-grained plagioclase, actinolite, chlorite, quartz, minor epidote, hematite, ilmenite.

mafic rocks, and that of La in the serpentinites and a few peridotites, imply that Cu behaves in a mobile manner while La is selectively mobile (Fig. 5I, J). Nd and Gd appear to be relatively less mobile except in two serpentinite samples which show scattering (Fig. 5K, L).

The chondrite-normalized REE patterns of the silicate-rich chromitites, serpentinites, and anorthosites are flat with low REE abundances (Fig. 6A). The peridotite show moderate enrichment in REE and have an HREE fractionated pattern ($Gd_N/Yb_N \approx 0.66–0.74$; Fig. 6A). The chromitites and serpentinites show strong negative Eu anomalies (Eu $anomaly_{chromitite} \approx 0.22–0.37$; Eu $anomaly_{serpentinite} \approx 0.22–0.63$; Fig. 6A) owing to hydrothermal alteration (e.g., Arndt et al., 1989). Positive Eu anomalies in the peridotite, anorthosites, and gabbro are due to the presence of plagioclase in these rocks (Eu $anomaly_{peridotite} \approx 1.34$; Eu $anomaly_{anorthosite} \approx 1.42–1.58$; Fig. 6A, B). Relative to the previously analyzed chromitites (Mukherjee et al., 2012), the chromitites in this study have higher abundances of REE (Fig. 6A). This is because the

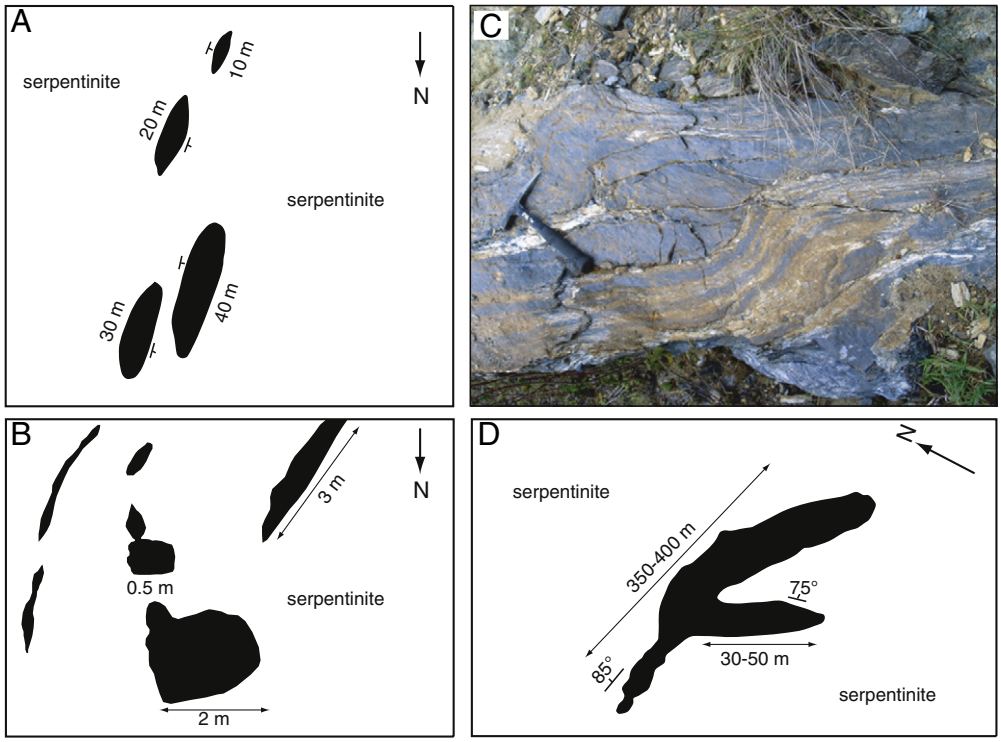

Fig. 3. Description of field occurrences of chromitite orebodies hosted within deformed serpentinite in the Nuggihalli greenstone belt. (A) Lenticular occurrences of chromitite orebodies (now represented by ponds in the mines; length 10–50 m, width 0.5–2 m) in the Tagdur mine. Orebodies mainly have a N–S to NE–SW trend with 75–85° dip towards the E. (B) Stringers and pods of chromitite occurring within serpentinite in the Tagdur mine. (C) Distinctly folded chromitite body within serpentinite in the Aladahalli mine. (D) Folded orebody (mined) mainly showing an E–W trend towards the N in the Tagdur mine. Part of the body shows variation in trend from NW–SE towards the E.

Table 4c
Major element data on anhydrous basis (wt.%) and trace element (ppm) data of samples from the Nuggihalli greenstone belt.

	DHR-10-100 chromitite	DHR-10-123 chromitite	DHR-10-119 serpentinite	DHR-10-93 peridotite	DHR-10-94 peridotite	DHR-10-96 peridotite	DHR-10-103 pyroxenite	DHR-10-106 pyroxenite	DHR-10-44 magnetite	DHR-10-107 gabbro	DHR-10-108 gabbro	DHR-10-110 gabbro	DHR-10-115 gabbro	DHR-10-116 gabbro	DHR-10-84 komatiitic schist	DHR-10-85 komatiitic basalt schist	DHR-10-88 komatiitic basalt schist	DHR-10-91 komatiitic basalt schist
wt.%																		
SiO_2			40.37	45.97	47.56	46.00	45.68	35.36		38.37	37.35	44.96	45.64	46.30	34.27	50.97	51.55	53.15
Al_2O_3			1.91	6.84	7.03	6.40	6.50	15.70		19.27	16.22	11.36	11.38	11.97	13.36	10.49	13.59	13.33
TiO_2			0.08	0.20	0.18	0.16	0.28	2.62		1.63	1.57	2.04	2.08	1.86	0.19	1.24	2.00	1.58
Fe_2O_3			13.89	10.66	8.89	9.11	14.25	27.64		21.16	22.89	20.36	17.38	16.99	13.73	14.34	11.93	11.02
MnO			0	0.02	0.03	0.08	0.17	0.20		0.14	0.17	0.19	0.27	0.25	0.15	0.19	0.15	0.11
MgO			43.66	29.36	25.55	30.73	23.90	16.92		8.34	11.40	7.61	8.98	8.30	33.07	9.91	6.62	6.90
CaO			0.08	6.89	10.53	7.48	9.19	1.38		9.51	8.81	12.32	12.85	12.58	5.16	9.31	10.33	9.72
Na_2O			0	0.05	0.22	0.04	0.02	0.01		1.52	1.46	1.00	1.31	1.64	0.05	3.22	2.89	3.46
K2O			0	0	0.01	0.00	0	0		0.08	0.10	0.10	0.10	0.09	0.00	0.18	0.19	0.20
P2O5			0.01	0.01	0.00	0	0.01	0.17		0.02	0.03	0.06	0.02	0.02	0.01	0.14	0.75	0.53
LOI			22.40	4.57	2.64	3.85	3.95	7.89		4.78	3.49	1.93	1.98	1.78	6.97	1.02	0.98	0.75
ppm																		
Sc	6.79	6.06	6.78	22.94	22.41	16. 69	25.05	25.40	3.71	17.83	19.05	58.54	61.03	57.78	18.47	44.41	19.42	18.42
V	763.29	478.45	71.13	140.66	120.54	112.28	115.29	318.86	0.24	883.19	790.40	736.63	344.60	311.74	140.49	283.16	349.51	354.12
Cr	132615	122038	12868	4721	5415	2990	439.72	90.04	0.19	71.62	92.77	88.48	63.48	49.53	2019.73	532.44	229.07	267.96
Co	205.35	248.01	100.83	58.74	43.88	59.51	89.82	118.62	79.72	81.79	96.76	57.92	45.63	43.06	80.14	72.52	31.02	31.74
Ni	425.15	948.73	1226	388.38	257.17	426.93	533.28	150.82	51.60	157.74	165.73	17.65	11.16	6.96	920.73	158.35	85.62	57.38
Cu	26.39	15.88	24.62	29.47	20.56	20.23	81.20	373.76	38.51	621.62	677.97	147.96	39.24	29.85	18.28	41.88	34.44	33.39
Zn	647.04	1066	125.98	19.29	13.93	18.98	99.70	153.24	48.44	106.91	121.38	113.03	118.66	100.17	42.90	86.89	60.96	35.11
Ga	33.70	12.23	3.22	7.02	5.57	5.08	4.90	15.43		26.72	21.38	20.59	16.74	16.76	8.67	17.16	21.28	23.63
Rb	0.5	0.93	0.41	0.23	0.41	0.23	0.23	0.18	0.53	0.76	0.85	0.74	1.14	0.85	0.39	4.44	0.93	4.12
Sr	1.662	1.25	0.89	1.60	2.47	1.95	12.53	12.06	9.10	248.75	157.37	182.33	125.27	178.85	4.11	169.10	49.23	60.92
Y	1.24	0.54	0.51	5.24	4.67	3.94	7.35	7.08	0.20	5.45	5.09	17.25	13.14	12.52	4.20	21.65	51.95	67.76
Zr	0.48	0.12	0.14	1.91	1.65	2.28	9.52	21.58	827.69	8.46	14.10	17.65	13.04	8.62	1.15	114.32	10.38	31.15
Nb	0.07	0.06	0.01	0.07	0.03	0.05	0.35	5.09	5.73	1.01	0.82	1.32	0.57	0.55	0.02	6.28	1.38	2.15
Cs	0.04	0.05	0.02	0.04	0.04	0.02	0.03	0.04	0.02	0.04	0.04	0.07	0.06	0.04	0.06	0.53	0.06	0.05
Ba	3.70	4.53	1.96	1.06	1.94	1.85	6.98	10.39	27.17	18.77	15.24	13.08	14.46	10.83	3.23	10.75	7.09	13.28
Hf	0.01	0.003	0.004	0.05	0.05	0.07	0.22	0.53	0.02	0.24	0.35	0.51	0.41	0.29	0.04	2.60	0.27	0.79
Ta	0.01	0.01	0.001	0.15	0.03	0.05	0.11	0.24	3.33	0.09	0.11	0.09	0.10	0.04	0.01	0.28	0.21	0.31
Pb	3.23	2.87	4.32	3.44	3.22	3.03	4.21	2.53	2.16	1.72	2.15	2.12	2.71	1.54	3.12	3.04	5.35	4.46
Th	0.06	0.08	0.04	0.04	0.02	0.03	0.12	0.27	0.07	0.18	0.18	0.16	0.10	0.07	0.02	1.27	0.77	1.09
U	0.03	0.04	0.02	0.04	0.04	0.03	0.22	0.09	0.003	0.04	0.16	0.1	0.11	0.01	0.08	0.25	0.29	0.27
La	0.39	0.63	0.37	0.60	0.42	0.53	0.31	2.00	0.17	1.75	1.28	1.96	0.96	0.96	0.26	8.49	12.00	17.77
Ce	0.37	1.23	0.85	0.89	0.54	1.004	0.65	18.35	0.39	3.46	2.53	4.41	2.38	2.31	0.57	18.75	27.60	39.11
Pr	0.12	0.18	0.11	0.16	0.14	0.19	0.11	0.80	0.04	0.54	0.41	0.82	0.46	0.45	0.09	2.60	4.48	6.20
Nd	0.53	0.73	0.56	0.86	0.78	0.97	0.71	3.67	0.13	2.58	2.01	4.70	2.86	2.83	0.52	12.32	22.77	31.18
Sm	0.12	0.14	0.14	0.28	0.29	0.30	0.40	1.08	0.03	0.66	0.58	1.63	1.12	1.11	0.17	3.44	6.44	8.30
Eu	0.04	0.05	0.01	0.08	0.23	0.10	0.05	0.46	0.01	0.47	0.36	0.79	0.72	0.76	0.82	1.26	2.16	2.51
Gd	0.19	0.15	0.12	0.51	0.48	0.45	0.60	1.14	0.04	0.73	0.65	2.02	1.49	1.45	0.34	3.67	8.75	11.34
Tb	0.03	0.02	0.02	0.10	0.10	0.08	0.16	0.22	0.01	0.14	0.12	0.43	0.33	0.30	0.07	0.70	1.49	1.87
Dy	0.17	0.09	0.08	0.67	0.63	0.53	0.92	1.12	0.05	0.72	0.64	2.30	1.79	1.70	0.53	3.28	8.32	10.35
Ho	0.04	0.02	0.02	0.18	0.16	0.14	0.21	0.23	0.01	0.15	0.14	0.49	0.37	0.37	0.15	0.63	1.94	2.45
Er	0.14	0.07	0.07	0.59	0.55	0.47	0.72	0.73	0.03	0.51	0.47	1.60	1.22	1.17	0.49	1.98	5.69	7.30
Tm	0.03	0.01	0.02	0.11	0.10	0.08	0.11	0.11	0.003	0.08	0.07	0.23	0.17	0.17	0.09	0.28	0.92	1.22
Yb	0.13	0.08	0.10	0.63	0.57	0.49	0.70	0.67	0.02	0.47	0.45	1.45	1.08	1.02	0.51	1.64	4.89	6.61
Lu	0.02	0.01	0.02	0.11	0.10	0.08	0.10	0.10	0.004	0.07	0.07	0.21	0.16	0.16	0.08	0.25	0.76	1.02

Major element data from CESS (India); trace element data from NGRI (India); LOI values are shown for information purpose.

Table 5c
Platinum-group element data (ppb) of samples from the Nuggihalli greenstone belt.

	Lithology	Os	Ir	Ru	Rh	Pt	Pd	Pd/Ir	Pd/Pt	∑PGE
DHR-10-100	chromitite	84.8	37.4	101	8.80	21.0	43.2	1.16	2.06	296
DHR-10-123	chromitite	12.4	6.20	44.4	7.60	5.80	19.4	3.13	3.35	95.8
DHR-07-21[a]	serpentinite		2.23	11.6	0.90	0.76	0.87	0.39	1.14	16.4
DHR-07-23[a]	serpentinite		2.44	18.6	1.19	1.09	1.59	0.65	1.46	24.9
DHR-07-24[a]	serpentinite		0.78	3.98	0.27	0.14	0.61	0.79	4.26	5.78
DHR-07-30A[a]	serpentinite		5.07	50.3	3.15	0.42				59.0
DHR-07-30B[a]	serpentinite		7.40	47.5	4.88	0.17	0.51	0.07	3.09	60.4
DHR-07-36[a]	serpentinite		5.34	30.3	1.04	0.13	0.67	0.13	5.38	37.4
DHR-10-119	serpentinite	3.80	1.40	9.40	1.00	1.40	7.80	5.57	5.57	24.8
DHR-10-92	peridotite	1.00	0.60	4.00	2.00	9.00	13.0	21.7	1.44	29.6
DHR-10-93	peridotite	0.60	0.40	3.60	0.80	3.00	8.60	21.5	2.87	17.0
DHR-10-94	peridotite	4.60	1.40	3.80	1.00	4.00	5.40	3.86	1.35	20.2
DHR-10-95	peridotite	0.60	1.00	3.80	3.40	16.6	16.6	16.6	1.00	42.0
DHR-10-96	peridotite	0.80	0.60	1.40	0.60	2.40	8.40	14.0	3.50	14.2
DHR-10-99	peridotite	0.40	0.60	1.40	0.60	2.20	3.80	6.33	1.73	9.00
DHR-07-26[a]	pyroxenite		0.39	1.29	0.39	2.67	2.12	5.40	0.79	6.86
DHR-10-103	pyroxenite	1.20	0.60	2.00	1.40	11.2	18.6	31.0	1.66	35.0
DHR-10-106	pyroxenite	0.20	0.20	0.40	1.20	8.80	8.40	42.0	0.96	19.2
DHR-07-25[a]	magnetite		0.02	0.05	0.01	0.31	1.43	81.1	4.61	1.82
DHR-07-35[a]	gabbro		0.01	0.01	0.01	0.22	0.22	46.9	1.02	0.46
DHR-10-43	gabbro	0.20	0.20	0.80	0.60	1.80	5.60	28.0	3.11	9.20
DHR-10-107	gabbro	0.20	0.20	0.40	2.20	2.60	8.60	43.0	3.31	14.2
DHR-10-108	gabbro	0.20	0.20	0.40	0.60	5.00	4.40	22.0	0.88	10.8
DHR-10-109	gabbro	0.20	0.20	0.40	0.60	2.60	10.8	54.0	4.15	14.8
DHR-10-110	gabbro	0.20	0.00	0.40	0.40	0.80	7.80		9.75	9.60
DHR-10-114	gabbro	0.20	0.20	0.60	0.40	2.40	6.40	32.0	2.67	10.2
DHR-10-115	gabbro	0.20		0.20	0.40	1.20	11.2		9.33	13.2
DHR-10-116	gabbro	0.00		0.40	1.00	3.20	5.00		1.56	9.60
DHR-10-129	anorthosite	1.40	0.80	0.60	0.40	2.20	6.20	7.75	2.82	11.6
DHR-10-130	anorthosite	1.80	2.40	1.80	2.60	11.8	15.6	6.50	1.32	36.0
DHR-07-33[a]	komatiitic basalt schist		0.02	0.05	0.01	0.15	0.13	7.70	0.86	0.35
DHR-07-34[a]	komatiitic basalt schist		0.14	0.26	0.14	3.70	3.20	22.7	0.86	7.44
DHR-07-37[a]	komatiitic schist		1.12	5.27	0.58	6.84	9.14	8.13	1.34	23.0
DHR-07-38[a]	komatiitic basalt schist		0.10	0.07	0.08	1.69	1.07	10.7	0.63	3.01
DHR-10-84	komatiitic schist	0.80	0.60	3.60	1.40	8.80	12.0	20.0	1.36	27.2
DHR-10-85	komatiitic basalt schist	0.20	0.00	1.00	0.40	0.60	4.60		7.67	6.80
DHR-10-88	komatiitic basalt schist	0.20	0.20	0.60	1.00	5.00	5.20	26.0	1.04	12.2
DHR-10-91	komatiitic basalt schist	0.20	0.40	0.60	0.60	5.60	6.20	15.5	1.11	13.6

[a]Analysis from State Key Laboratory of Ore Deposit Geochemistry (SKLODG), Guiyang (China); rest of the analysis from NGRI, Hyderabad (India).

chromitites of the present study (e.g., DHR-10-100 and DHR-10-123) are silicate-rich (50 modal % chromite) relative to the previous ones that were massive (>75 modal % chromite). The interstitial silicates (now altered to serpentine and chlorite) contribute to the abundances of REEs as chromites do not host the rare earth elements. The pyroxenite, gabbro and metavolcanic schists show superchondritic REE abundances (Fig. 6B, C), exceptions being the komatiitic schists (DHR-07-37, DHR-10-84) that show subchondritic abundances of REE and an LREE depleted pattern ($La_N/Sm_N \approx 0.52–0.96$; Fig. 6C).

The effect of crustal contamination in the sill-like ultramafic–mafic rocks and the metavolcanic schists has been illustrated through binary variation diagrams in Fig. 7. The tonalite–trondhjemite–granodiorite rocks (Fig. 2) represent the Archean crust hence their field has been depicted in the figure. In the La versus Sm diagram (Fig. 7A) a positive correlation is observed, where the majority of the rocks plot closer to the primitive mantle line. The Nuggihalli rocks scatter closely about the primitive mantle line in the Th versus Yb plot (Fig. 7B) and the Zr versus TiO_2 diagram (Fig. 7C). The scattering is an outcome of mobility of these elements during secondary alteration.

4.2. Platinum-group elements

The platinum-group of elements and their ratios have been plotted against MgO in Fig. 8. In this figure, Ir and Ru show a distinct positive relation with MgO. The serpentinites and peridotites show a range of values from 0.4–7.4 ppb Ir and 1.8–50.3 ppb Ru (Table 5c). Anorthosite, gabbro, pyroxenite and metavolcanic schists show slight dispersion, and display a lower range from 0.005–1.12 ppb Ir and 0.007–5.27 ppb Ru (Fig. 8A, B; Table 5c). Pd and Pt exhibit a negative relation with MgO for the serpentinites and peridotites, while the pyroxenites, gabbro and metavolcanic schists show a contrastingly positive pattern (Fig. 8C, D). The cumulate gabbros and metavolcanic schists have a range of Pd and Pt values that are equivalent to the values in the peridotites and serpentinites (Table 5c). The Pd/Ir, Ru/Ir, and Pd/Pt ratios which reflect the fractionation between the platinum-group of elements (Barnes et al., 1985) have also been plotted against MgO (Fig. 8E–F). Pd/Ir conforms to the negative trend shown individually by Pd and Pt with MgO (Fig. 8C–D, F). Pd/Pt and Ru/Ir show an overall positive relation with MgO where the gabbros show high inter-sample variation for the former ratio (Fig. 8E, G). All the rocks of the ultramafic–mafic unit and the surrounding metavolcanic schists show a negative relation of Pd/Ir with Ni/Cu (Fig. 8H). Serpentinites show the least fractionation of the PGEs (Pd/Ir ≈ 0.07–0.79) with a few exceptions, along with the chromitites (Pd/Ir ≈ 1.15–3.12) both of which have higher Ni/Cu ratios (16.11–59.76 and 10.28–6220 respectively). The peridotites, anorthosites, pyroxenites, gabbros and metavolcanic schists show well fractionated PGE patterns (Pd/Ir ≈ 3.85–81.08) and low Ni/Cu ratios (0.11–115.87). IPGEs, namely Ir, Os and Ru show well-defined positive correlations with Cr, despite their slight dispersion observed in some rocks (Fig. 8I–K). In contrast, no correlation exists with Pt and Pd (Fig. 8L). The majority of the ultramafic–mafic rocks show higher Pd/Ir ratio compared to the primitive mantle (3.1–81.1; Pd/Ir_{PM} 1.2) (Fig. 9A), except for one chromitite sample that shows a primitive mantle value and the serpentinites that show sub-chondritic Pd/Ir (0.07–0.79). Pt and Pd are positively correlated in the ultramafic–mafic rocks, and the

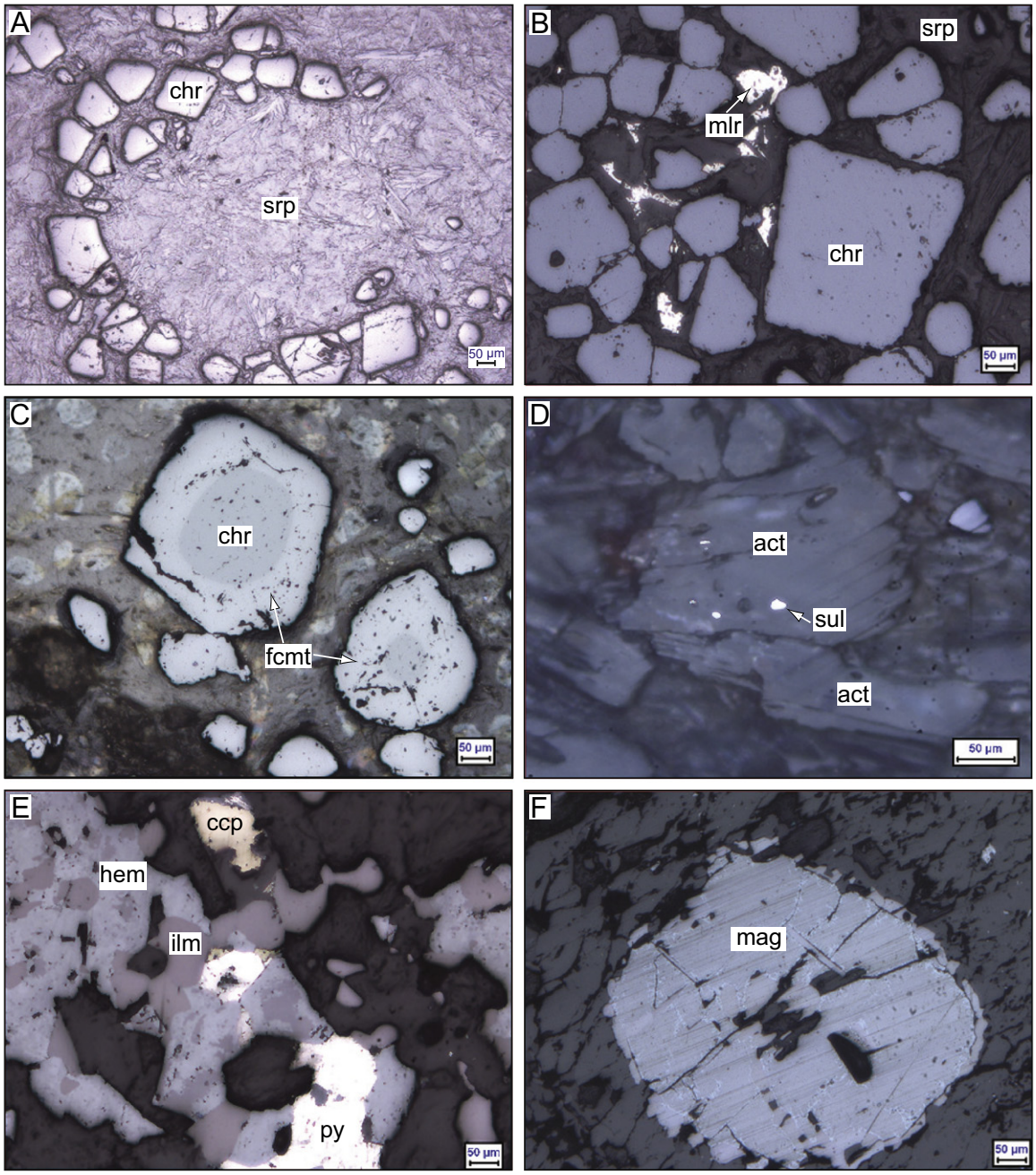

Fig. 4. Photomicrographs in reflected light of: (A) net-texture chromitite where chromite (chr) grains surround serpentine (srp) that have replaced earlier cumulus olivine; (B) massive chromitite with disseminated millerite (mlr) in the interstitial spaces; (C) altered chromite in silicate-rich chromitite exhibiting compositional zoning with ferritchromit rims (fcmt) and modified core; (D) altered pyroxenite comprising actinolite (act) with inclusions of sulfides (sul); (E) magnetite altered to ilmenite (ilm) and hematite (hem) with interstitial sulfides of chalcopyrite (ccp) and pyrite (py); (F) coarse cumulus magnetite (mag) within gabbro. Mineral abbreviations from Whitney and Evans (2010).

trend is approximately parallel to the primitive mantle (Fig. 9B), however, the serpentinites and gabbro show dispersion. Pd/Pt ratio is higher than primitive mantle in all of the rocks (0.63–9.75; Pd/Pt_{PM} 0.55).

Among the ultramafic plutonic rocks the chromitites are enriched in PGEs (total PGE ≈ 296.2–95.8 ppb; Table 5c). In the primitive-mantle normalized PGE diagram the chromitites have enriched Ru and Rh (≈8.8–20 × primitive mantle), where Pd/Ir ranges from primitive mantle-like values (Pd/Ir ≈ 1.2, Table 5c; Pd/Ir_{PM} ≈ 1.22; McDonough and Sun, 1995) to higher values of 3.1 (Table 5c; Fig. 10A). The serpentinites have low total PGE concentrations (5.8–60.4 ppb) and show IPGE enriched patterns with positive Ru anomaly, except for one sample (DHR-10-119) that is PPGE enriched with high Pd concentrations (≈1.3–2 × primitive mantle) relative to Ir (≈0.1–0.4 × primitive mantle) (Fig. 10A). In contrast to the serpentinites, the peridotites show PPGE enriched pattern with high Pd concentrations (1.0–4.3 × primitive mantle). The anorthosites also have PPGE enriched pattern with high Pd concentrations (1.6–4 × primitive mantle) relative to Ir (0.25–0.75), and a negative Ru anomaly (Fig. 10A). The total PGE concentrations in the peridotites (9–42 ppb) and anorthosites (11.6–36 ppb) are comparable to, if not slightly less than, those of the serpentinites (Table 5c). All the ultramafic plutonic rocks show a common feature in the primitive-mantle normalized diagram (Fig. 10A) i.e. they exhibit a distinct negative Pt anomaly, especially the serpentinites that show the greatest depletion in Pt; the majority of the rocks also show a negative Ir anomaly (Fig. 10A).

The gabbro and pyroxenites show strong PPGE enriched patterns but are characterized by lower PGE concentrations ($\sum PGE_{pyroxenite}$ 6.9–35 ppb; $\sum PGE_{gabbro}$ 0.46–14.8 ppb) compared to the ultramafic plutonics (Fig. 10A, B; Table 5c). The majority of the gabbros, except for one sample (DHR-07-35) which has the lowest concentration of total PGE, show higher Rh and Pd concentrations (Rh: 0.4–2.4 × primitive mantle; Pd: 1.1–2.9 × primitive mantle; Fig. 10B) than the rest of the platinum-group elements. The magnetite shows PPGE enriched pattern and low PGE concentrations similar to the gabbro DHR-10-35.

The metavolcanic schists also have PPGE enriched PGE patterns, with total PGE concentrations in the range of the gabbros (0.35–27.2 ppb; Fig. 10C; Table 5c). Pt concentrations are low in the rocks especially in one of the komatiitic basalt schist (DHR-10-85) that shows a deep negative anomaly of Pt, while another (DHR-07-38) shows a distinct negative Ru anomaly.

5. Discussion

5.1. Parental magma and formation of the ultramafic–mafic complex

The parental magma and magmatic fractionation history of the sill-like ultramafic–mafic plutonic rocks and the surrounding metavolcanic schists in the Nuggihalli greenstone belt have been described in Mukherjee et al. (2012). A brief summary is provided below. The metavolcanic schists and plutonic ultramafic–mafic rocks (Fig. 2) experienced fractional crystallization, based on the similarity in their major

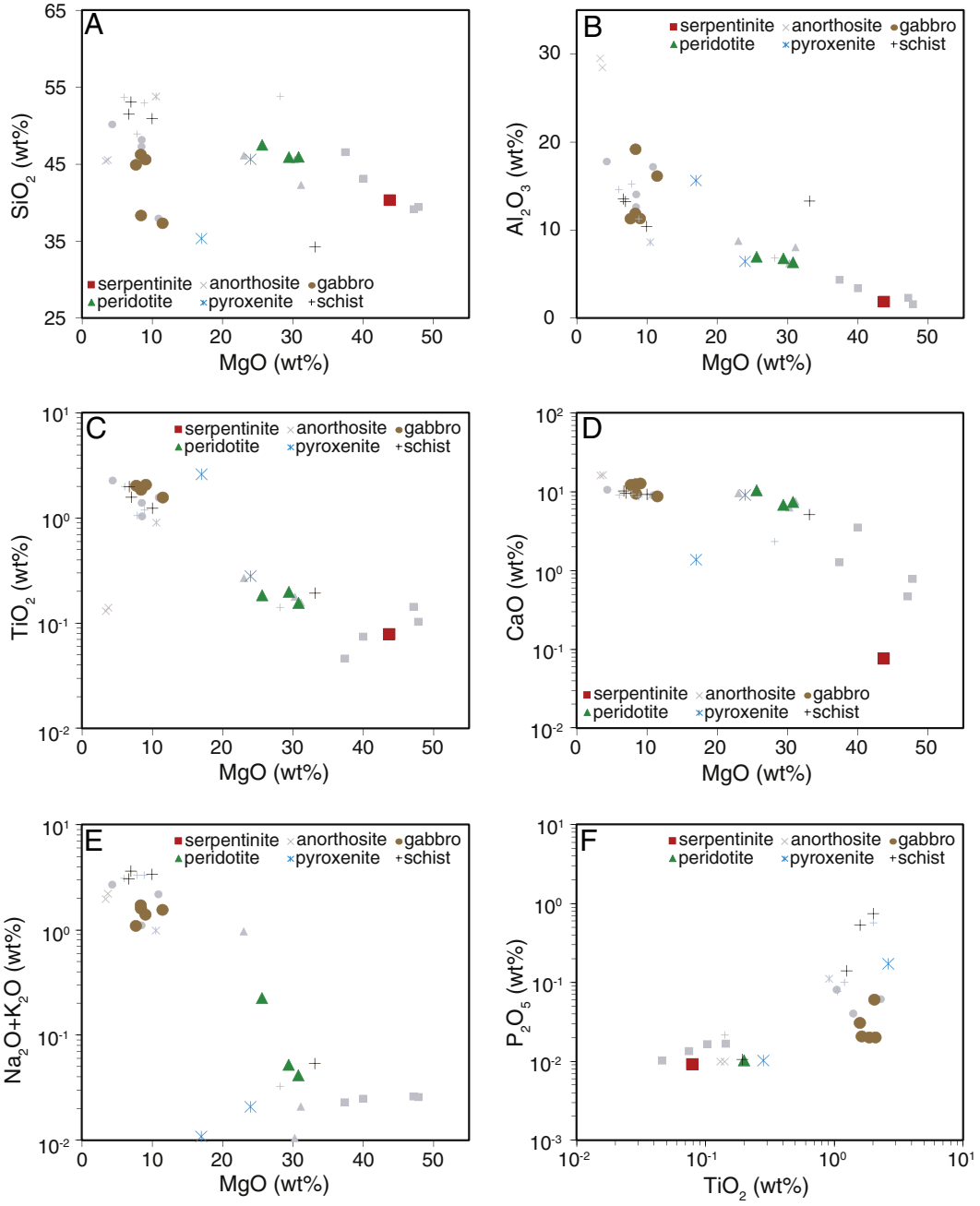

Fig. 5. Variation diagrams for selected major (anhydrous basis) and trace elements (A) MgO versus SiO_2, (B) MgO versus Al_2O_3, (C) MgO versus TiO_2, (D) MgO versus CaO, (E) MgO versus $Na_2O + K_2O$, (F) TiO_2 versus P_2O_5, (G) MgO versus Ni, (H) MgO versus Cr, (I) MgO versus Cu, (J) MgO versus La, (K) MgO versus Gd, and (L) MgO versus Nd. Data of samples from the Nuggihalli greenstone belt published in Mukherjee et al. (2012) are indicated in gray, sample legends remain unchanged.

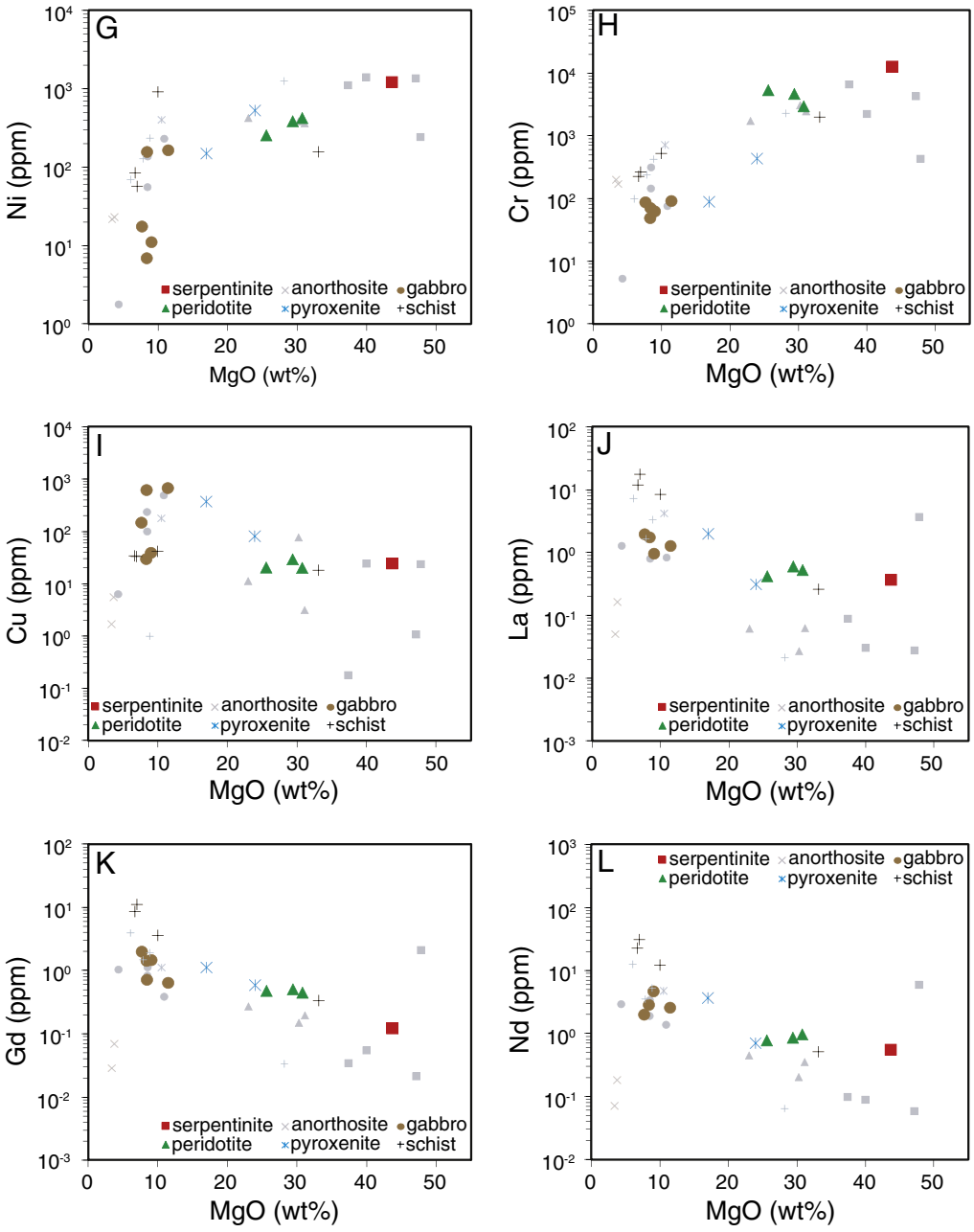

Fig. 5 (*continued*).

and trace element data with the fractionation trend of komatiites to komatiitic basalt reported from the Western Dharwar craton by Jayananda et al. (2008). Al-depleted komatiite was inferred to be the parental magma of the ultramafic–mafic rocks, based on similarity of the chondrite-normalized REE pattern of the metavolcanic schists with Al-depleted komatiites from the Western Dharwar craton (e.g., Jayananda et al., 2008), and the Barberton greenstone belt (e.g., Arndt et al., 2008). This is consistent with the inference that low-Al komatiitic basalt was the parental magma of the chromitites, based on unaltered chromite composition from massive chromitites (Mukherjee et al., 2010). The Al-depleted komatiites were derived from a depleted mantle source based on positive ε_{Nd} values of the ultramafic–mafic plutonic and volcanic rocks (+1.7 to +3.4), and the low initial Sr isotope value of the gabbros (0.70097–0.70111). Tectonic discrimination diagrams based on unaltered chromites indicated derivation of the komatiites from a supra-subduction zone setting, where the komatiites were generated by melting of the depleted mantle wedge (Mukherjee et al., 2010). The MELTS program of Ghiorso and Sack (1995) was utilized to show that fractionation of an Al-depleted komatiite (e.g., Jayananda et al., 2008) at 1638 °C, 2Kbar and fO_2 at QFM could produce a sequence of crystallization of minerals that matched with the plutonic ultramafic–mafic rock sequence in the Nuggihalli greenstone belt. We thus inferred that the protoliths of the metavolcanic and plutonic suites were contemporaneous (3.1 Ga; Mukherjee et al., 2012), and formed from similar parental magmas that experienced parallel fractionation from komatiite to a komatiitic basalt. The sill-like ultramafic–mafic rocks may have been the plutonic equivalents of the metavolcanic

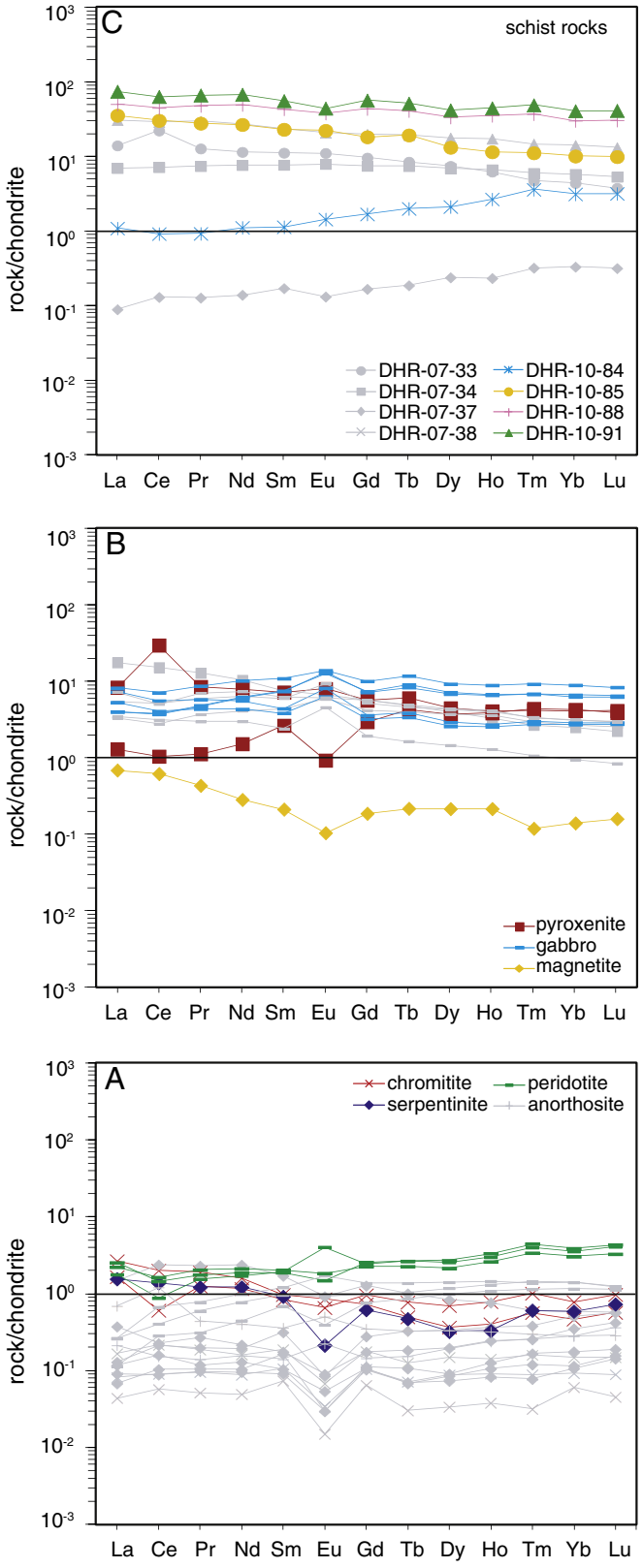

Fig. 6. Chondrite-normalized REE diagrams of (A) chromitite, serpentinite, peridotite, and anorthosite; (B) pyroxenite and gabbro; and (C) metavolcanic schist rocks from the Nuggihalli greenstone belt. Normalized chondrite values from McDonough and Sun (1995). Komatiitic schist: DHR-07-37 and DHR-10-84; Komatiitic basalt schist: DHR-07-33, DHR-07-34, DHR-07-38, DHR-10-85, DHR-10-88 and DHR-10-91. Data of samples from the Nuggihalli greenstone belt published in Mukherjee et al. (2012) are indicated in gray, sample legends remain unchanged.

schists with their present disposition being solely an outcome of later tectonic disturbances.

6.2. PGE fractionation and implications for the mantle source

The absolute concentration of the IPGEs (e.g., Ir and Ru) in the ultramafic–mafic rocks and their correlation with MgO and Cr (Fig. 8A, B, I–K) implies that both Ir and Ru were compatible and fractionated by the early crystallizing phases, namely chromite (e.g., Puchtel et al., 2004; Barnes and Fiorentini, 2008), or by Ir–Ru-bearing alloys hosted within these minerals. Progressive decrease in Ru/Ir ratio with MgO for the ultramafic plutonics followed by the pyroxenites, gabbro and schists (Fig. 8E) further implies that Ru was more compatible in chromite relative to Ir. Good correlations of Ir and Ru with Cr (Fig. 8J, K) are noted in all types of chromite occurrences like the Archean high-grade complexes, Archean greenstone belts, layered intrusions, ophiolites (e.g., Mathez, 1999 and references therein), and in komatiites and komatiitic basalts (e.g., Puchtel et al., 2004). Despite alteration and low-grade metamorphism in the rocks, the PGEs are immobile which is understood from the good correlation of PGEs with MgO, and the IPGEs with Cr (Fig. 8A–G, I–K). The negative trend displayed by the rocks of the ultramafic–mafic unit and the surrounding metavolcanic schists in the Pd/Ir and Ni/Cu plot (Fig. 8H), may be explained by olivine–chromite fractionation and accumulation in the early cumulates (e.g., Barnes et al., 1988). Olivine prefers Ni relative to Cu while chromite or included IPGE phases prefers Ir to Pd (Barnes et al., 1988), thus fractionation of these minerals results in lowering of the Ni/Cu ratio, and a sharp increase in Pd/Ir in the evolved differentiates. The metavolcanic schists DHR-07-37 and DHR-10-84 are komatiitic in composition (Mukherjee et al., 2012) and thus show high Ni/Cu ratio (31.38–50.37) owing to greater abundances of olivine, while the rest of the metavolcanic schists compositionally represent fractionated komatiitic basalts (Mukherjee et al., 2012) with low Ni/Cu ratios (Fig. 8H). The Pd/Ir ratio (0.07–0.79) in serpentinites is lower than that of the primitive mantle (Fig. 9A) due to their high Ir concentration which is related to the modal abundances of accessory chromite grains.

In the primitive-mantle normalized PGE diagram (Fig. 10A) the chromitites are either IPGE-enriched (e.g., DHR-10-100) or have flat PGE pattern with depletion in Pt (e.g., DHR-10-123). The chromitites are PGE-enriched compared to the host serpentinites and peridotites which is a common feature (e.g., Ahmed and Arai, 2002; Mondal and Zhou, 2010). PGE enrichment in chromitites, especially of the IPGEs, has been explained to be an outcome of either or both of the following: (a) structural compatibility of the IPGEs with chromite where they undergo ionic substitution and exhibit solid-solution (Capobianco and Drake, 1990; Peach and Mathez, 1996; Righter et al., 2004; Locmelis et al., 2011; Brenan et al., 2012) or (b) physical entrainment of IPGE-rich PGM or alloy phases as inferred from the presence of inclusions of nanometer to sub-millimeter sized laurite (RuS_2)–erlichmanite (OsS_2) solid solution, osmiridium (Os–Ir alloy) and isoferroplatinum (Pt_3Fe) within chromite grains (Tredoux et al., 1995; Sattari et al., 2002; Ballhaus et al., 2006). Apart from chromite, olivine was considered to play some role in PGE fractionation in komatiites based on the compatibility of IPGEs in their structure (e.g., Brügmann et al., 1987; Zhou, 1994; Rehkämper et al., 1999). However, based on recent experimental and mineral separate studies authors now prefer to explain this in terms of physical incorporation of IPGE alloys by the growing olivine crystal (e.g., Puchtel et al., 2004; Brenan et al., 2005; Puchtel and Humayun, 2005; Barnes and Fiorentini, 2008; Puchtel et al., 2009).

Enrichment of IPGE in massive chromitites of the Nuggihalli greenstone belt may be explained by the presence of inclusions of IPGE-rich platinum-group minerals (PGM), namely laurite and other IPGE-bearing sulfarsenides (e.g., Devaraju et al., 2007). An IPGE enriched pattern is also observed in the serpentinites from Nuggihalli, and is due to the presence of accessory chromites. The average primitive-mantle normalized PGE patterns of the chromitites have been compared with

komatiite-derived massive chromitites from the Archean Selukwe greenstone belt (Zimbabwe craton), PGE and sulfide-rich UG2 chromitite of the Bushveld Complex (South Africa), PGE unmineralized sulfide-poor massive chromitites from the G-chromitite of the Stillwater Complex (USA), and stratiform and podiform chromitites from the crust and mantle section of ophiolites (Oman ophiolite, UAE) (Fig. 11). The PGE pattern of the chromitites from our study shows a very close resemblance with the IPGE-enriched sulfide-poor massive chromitites from all occurrences (Fig. 11).

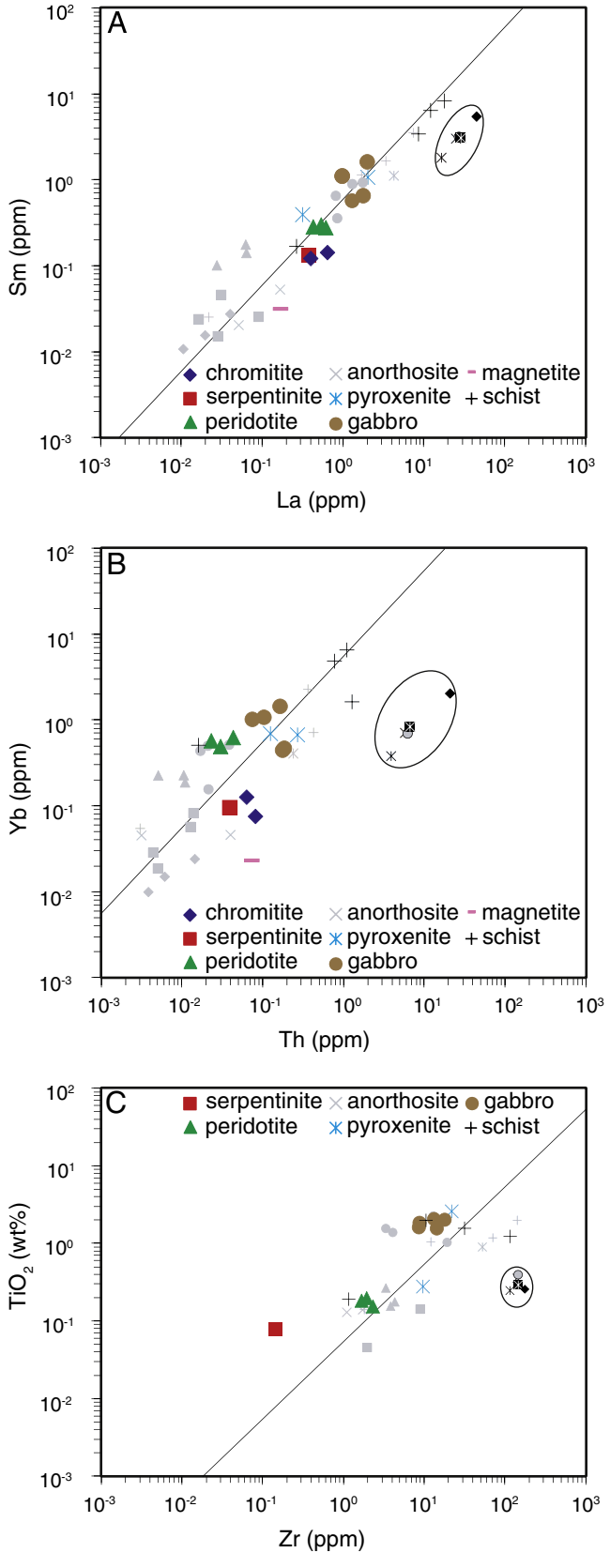

The negative Pt anomaly exhibited by the plutonic ultramafic rocks, a few gabbros and metavolcanic schists from our study (Fig. 10), also occurs in ultramafic–mafic rocks from the mantle and crustal sections in ophiolites (Zhou et al., 1998; Ahmed and Arai, 2002), peridotitic mantle xenoliths (Lorand et al., 2004) and the sulfides (interstitial and monosulfide solid solution) occurring within them (Alard et al., 2000; Lorand and Alard, 2001), as well as in Archean greenstone belt rocks (Mondal and Zhou, 2010). Pt depletion in mantle sulfides was explained to occur due to the tendency of Pt to form micro-nuggets either during serpentinization (under low oxygen fugacity; Alard et al., 2000), or as low-temperature exsolutions from pentlandites (Peach and Mathez, 1996; Lorand and Alard, 2001 and references therein). Experiments by Borisov and Palme (1997) showed Pt solubility in silicate melts to be strongly dependent on fo_2, where reducing conditions favor the formation of Pt nuggets. Pt depletion in most of the plutonic rocks from the Nuggihalli greenstone belt may be explained by fractionation of a Pt–Fe alloy in the early stages of magma generation. At this stage alloys will stabilize relative to sulfides because of low sulfur fugacity owing to the high temperature of the magma (Keays et al., 1981). Alternatively, Pt depletion may be a characteristic of the source mantle, where depletion occurs due to the presence of discrete nano-sized Pt nuggets that are difficult to be entrained by the magma during partial melting (Alard et al., 2000). Pt-depletion in the source may also be explained by the displacement of Pt-alloys to isolated deep-seated mantle domains that develop during crystallization of the primitive magma ocean, thus creating Pt-enriched and Pt-depleted mantle sources in the early Archean (Puchtel et al., 2014).

The PPGE enriched trend in the peridotites, anorthosites, pyroxenites, gabbro, and magnetite (Fig. 10A, B) can be explained by removal of IPGEs by the early-accumulated olivine and chromite minerals, and the incompatible nature of PPGEs during magma differentiation (e.g., Barnes et al., 1985). The komatiitic schists (e.g., DHR-07-37 and DHR-10-84) have less depleted PGE abundances than the komatiitic basalt ones (Fig. 10C). The PPGE enriched pattern of the metavolcanic schists implies retention of IPGE in the mantle source or IPGE alloy saturation in the melt (e.g., Fiorentini et al., 2011); incompatible behavior of the PPGEs is due to the sulfide-undersaturated nature of the source.

The PGE in the Nuggihalli metavolcanic schists have been normalized to 25 wt.% MgO, which is the representative MgO content in komatiites, and compared with early-, meso- and late Archean komatiites. The average primitive mantle-normalized PGE comparison plot is shown in Fig. 12. The early Archean komatiites are from the Barberton greenstone belt (3.4–3.5 Ga; Maier et al., 2009; Fiorentini et al., 2011 and references therein), the Mesoarchean ones are from the greenstone belts of Youanmi Terrane (2.9 Ga) in Western Australia (Fiorentini et al., 2011 and references therein) and the late Archean komatiites are from the 2.7 Ga Agnew-Wiluna greenstone belt and the greenstone belts of Kurnalpi Terrane in Western Australia (Fiorentini et al., 2011; Barnes et al., 2012 and references therein). The average PGE pattern of the Nuggihalli metavolcanic schists is observed to be similar to the pattern of early Archean Barberton komatiite (Komati Formation), except that it has significantly higher Ir and slightly higher abundances of Ru and Rh (Fig. 12). The low Ir abundances results in

Fig. 7. Plot of (A) La versus Sm, (B) Th versus Yb, and (C) Zr versus TiO_2 for the Nuggihalli ultramafic–mafic plutonics and associated metavolcanic schists. The line illustrates the primitive mantle (McDonough and Sun, 1995) ratio of the trace elements. Data of TTGs have been incorporated to check the crustal contamination status of the rocks. ⧓ Holenarsipur TTGs (Naqvi et al., 2009); × low pressure sodic TTG (Moyen and Martin, 2012); ⚹ high pressure low HREE sodic TTG (Moyen and Martin, 2012); ◍ high-pressure medium HREE sodic TTG (Moyen and Martin, 2012); ◆ potassic TTG (Moyen and Martin, 2012). Data of samples from the Nuggihalli greenstone belt published in Mukherjee et al. (2012) are indicated in gray, sample legends remain unchanged.

highly fractionated PGE patterns in the Barberton komatiite (Komati Formation) compared to the Nuggihalli metavolcanic schists ($Pd/Ir_N^{Barberton\ Komati} \approx 40.7$; $Pd/Ir_N^{Nuggihalli} \approx 6.3–21.3$). The average PGE pattern of the metavolcanic schists is also comparable to the PGE pattern of komatiite from Sandstone, except for the slightly higher Ir and Pt abundances in the latter (Fig. 12). The relatively younger komatiites from Western Australia are enriched in PGE compared to the early Archean and Mesoarchean ones (Fig. 12).

The PGE depleted character exhibited by the metavolcanic schists (compositionally komatiitic or komatiitic basalt) from the Nuggihalli greenstone belt is typical of early Archean komatiites relative to the late Archean ones (Maier et al., 2009; Fiorentini et al., 2011), however the PGE are more fractionated in the Nuggihalli metavolcanic schists (Fig. 12). PGE depletion was explained to be an outcome of core segregation (4.55 Ga), while the enrichment in late Archean komatiite sources was attributed by Maier et al. (2009) to progressive mixing of PGE-enriched cosmic material (compositionally chondrites) that accreted into the mantle during late heavy meteorite bombardment (≈4.5–3.8 Ga) (Late Veneer Theory; Chou, 1978). The mantle source of the plutonic ultramafic–mafic rocks and metavolcanic schists from our study has been inferred to be depleted based on the positive ε_{Nd} of the rocks (+1.7 to +1.34), and the low $^{86}Sr/^{88}Sr^{initial}$ ratio of the gabbro (0.70097–0.70111; Mukherjee et al., 2012). The depleted nature of komatiite sources in terms of their Sm–Nd isotope system is explained

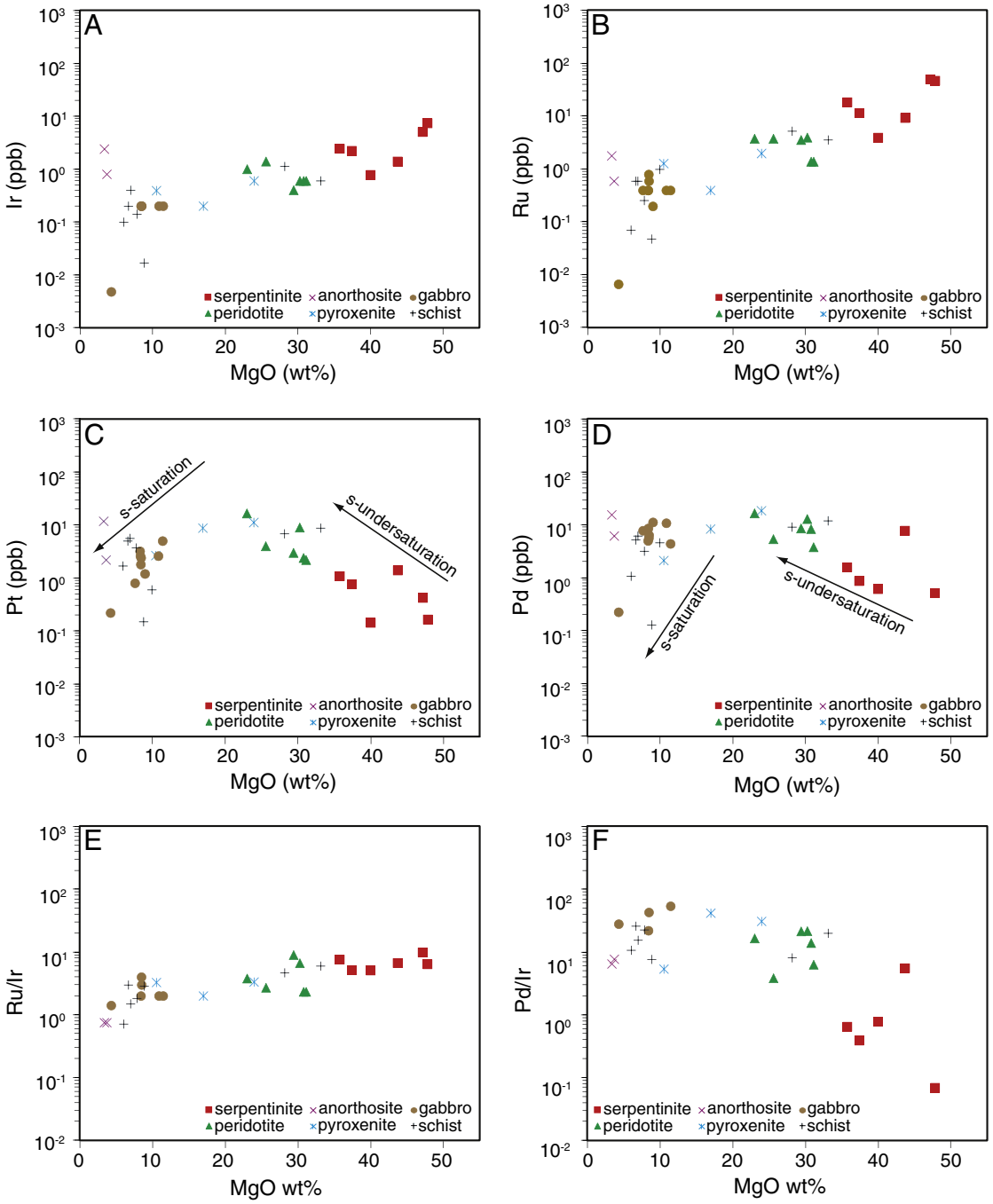

Fig. 8. (A) MgO versus Ir. (B) MgO versus Ru. (C) MgO versus Pt; trends of sulfide saturation and undersaturation have been illustrated. (D) MgO versus Pd; trends of sulfide-saturation and undersaturation have been illustrated. (E) MgO versus Ru/Ir. (F) MgO versus Pd/Ir. (G) MgO versus Pd/Pt. (H) Ni/Cu versus Pd/Ir; trends of primitive mantle melting (pmt), chromite addition (c.a.), chromite removal (c.r.), olivine addition (o.a.) and olivine removal (o.r.) from Barnes et al. (1988) have been shown. (I) Cr versus Os. (J) Cr versus Ir. (K) Cr versus Ru. (L) Cr versus Pd/Pt.

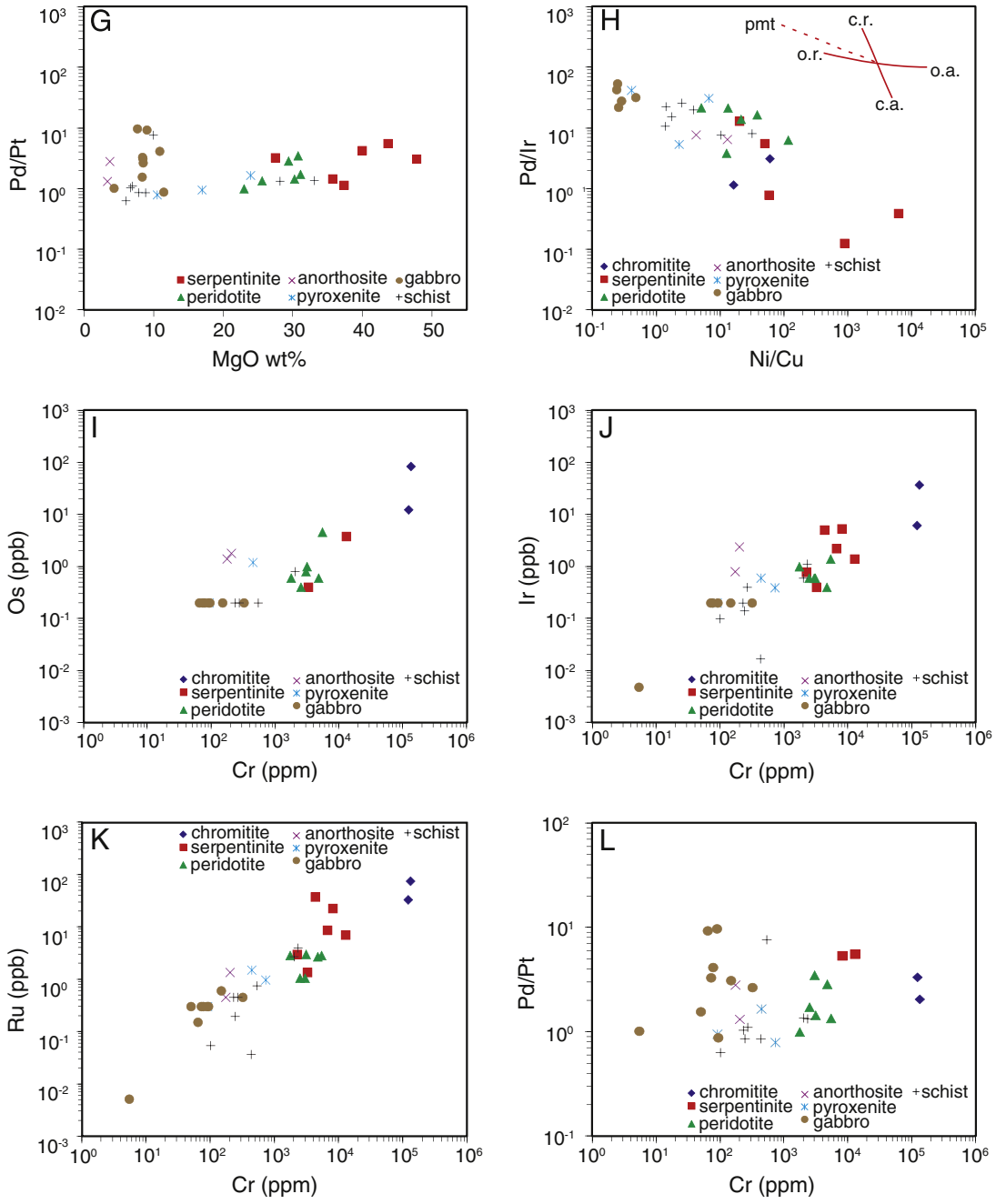

Fig. 8 (*continued*).

to be an outcome of crystallization of an initial magma ocean or extraction of the continental crust (Puchtel et al., 2009). However, the processes responsible for imparting PGE and Nd isotope depletion in the komatiite sources are considered to be independent of one another (Maier et al., 2009).

Recently Puchtel et al. (2014) studied the early Archean Barberton komatiites using integrated PGE, ^{142,143}Nd, Re–Os, Pt–Os and Lu–Hf isotopic systematics. In contrast to the findings of Maier et al. (2009), Puchtel et al. (2014) found no significant changes in PGE abundances between the early and late Archean komatiite sources that had similar Pt + Pd abundances. The authors noticed Pt fractionation in early Archean komatiite sources where Pt was either removed or added to the sources, compared to the late Archean ones. As opposed to downward mixing of a PGE-rich late veneer proposed by Maier et al. (2009), the Pt concentration variations in early Archean komatiites were explained by Puchtel et al. (2014) as dispersal of Pt alloys to lower mantle domains during the major silicate differentiation event, thereby creating Pt-enriched and Pt-depleted domains. In their view the deep-seated mantle domains had fractionated time-integrated Sm/Nd, Lu/Hf, and Pt/Os ratios (≈4.4 Ga), and were generated during crystallization of a primitive magma ocean with Mg-perovskite, Ca-perovskite, and Pt-alloy as the fractionating phases. The mantle domains remained isolated from the convecting mantle but mixed away by 2.7 Ga, as evidenced by uniform time-integrated Sm/Nd, Lu/Hf, and Pt/Os ratios of the late Archean komatiite systems that sampled these sources.

Pt fractionation is also observed among the metavolcanic schists from the Nuggihalli greenstone belt that show Pt depletion in one of the samples (e.g., DHR-10-85) compared to the rest (Fig. 10C). In Fig. 12, Pt

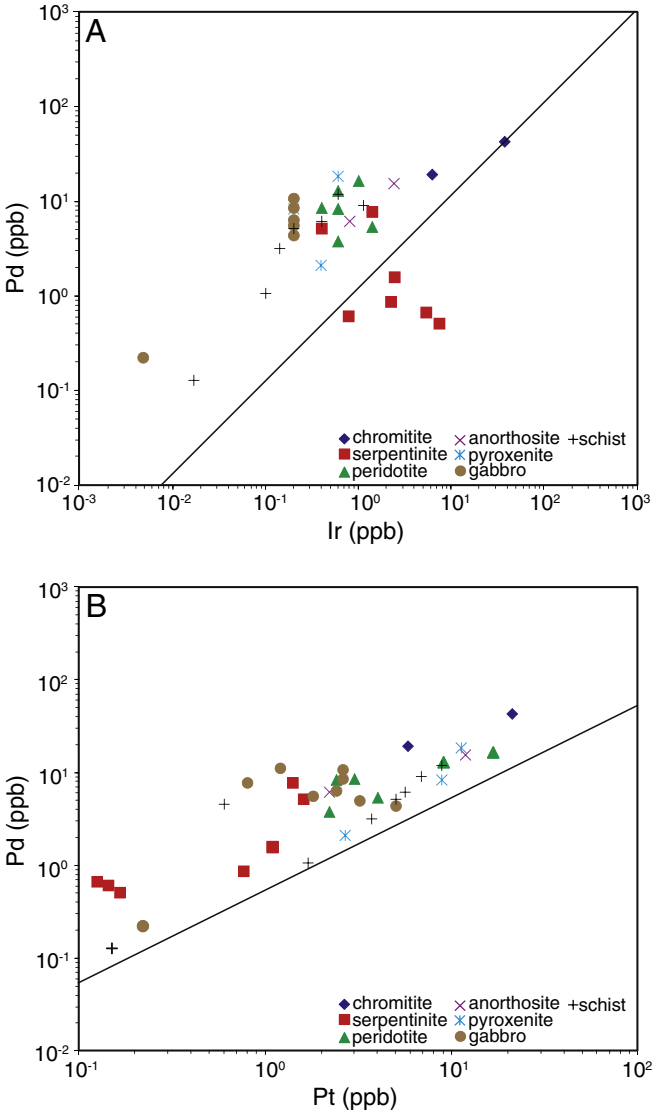

Fig. 9. (A) Ir versus Pd. (B) Pt versus Pd. The line illustrates primitive mantle (McDonough and Sun, 1995) ratio of the platinum-group elements.

depletion is found to be present in both the early Archean (Barberton komatiites–Weltverden Formation; Ravensthorpe–Youanmi Terrane) and late Archean komatiites (Murchison and Gindalbie Terrane). Thus in conclusion, the similarity of the whole-rock PGE patterns of the Nuggihalli metavolcanic schists with the PGE depleted character of early Archean komatiites agrees with the theory of slow progressive mixing (till 2.9 Ga) of the PGE-enriched chondritic late veneer matter in the Earth's mantle (Maier et al., 2009; Fiorentini et al., 2011). Comparison of PGE patterns of early and late Archean komatiites indicates that isolated Pt-enriched and Pt-depleted domains probably existed in the early Archean but it did not mix away by 2.7 Ga as has been proposed by Puchtel et al. (2014).

5.3. Sulfide saturation of the parental magma

In the plutonic suite pyroxenites (Fig. 2) mark the transition from sulfide-undersaturation to sulfide-saturation. This is clearly observed from the binary plots of MgO versus Pd, Pt and Pd/Ir (Fig. 8C–D, F). In the figure pyroxenites represent a break in trend from the negative correlation of Pd, Pt and Pd/Ir with MgO displayed by the serpentinites and peridotites due to incompatible behavior of the PPGEs, to the positive

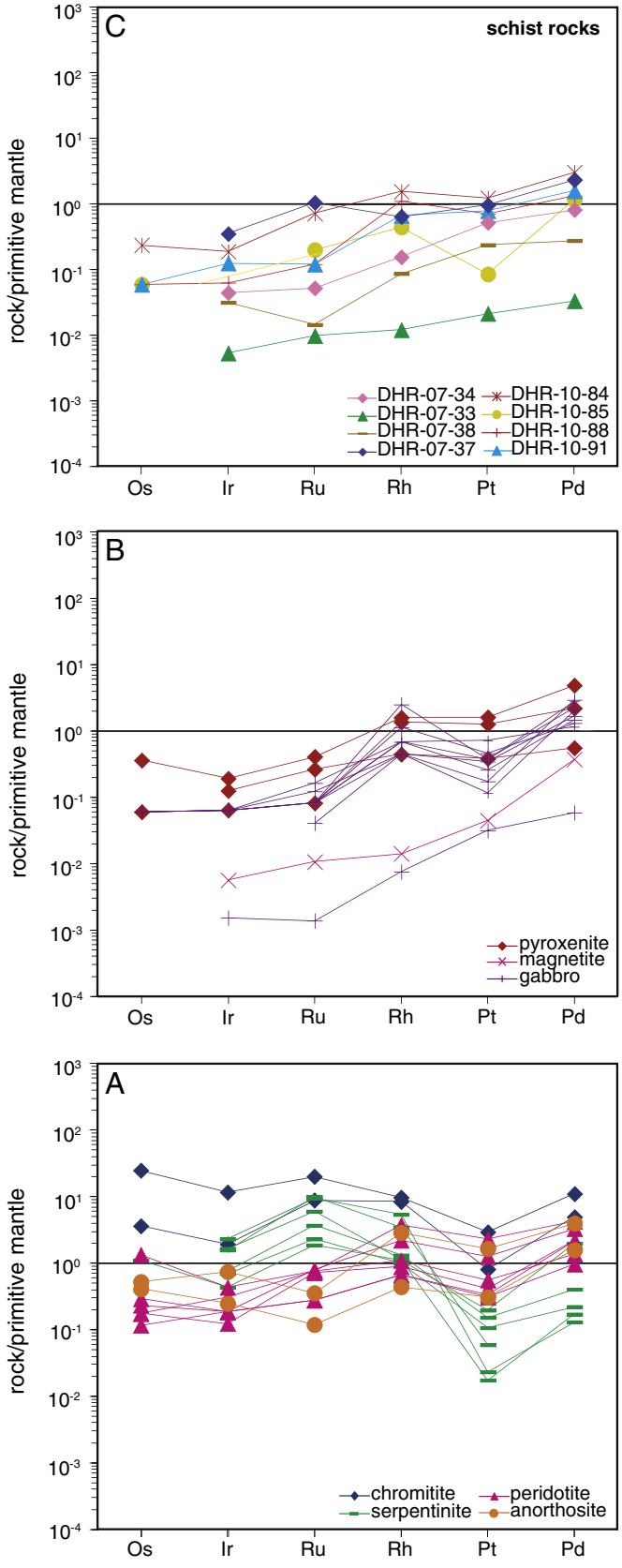

Fig. 10. Primitive mantle-normalized metal patterns for (A) chromitite, serpentinite, peridotite, and anorthosite; (B) pyroxenite, magnetite and gabbro (C) metavolcanic schist rocks; sample details as in Fig. 5.

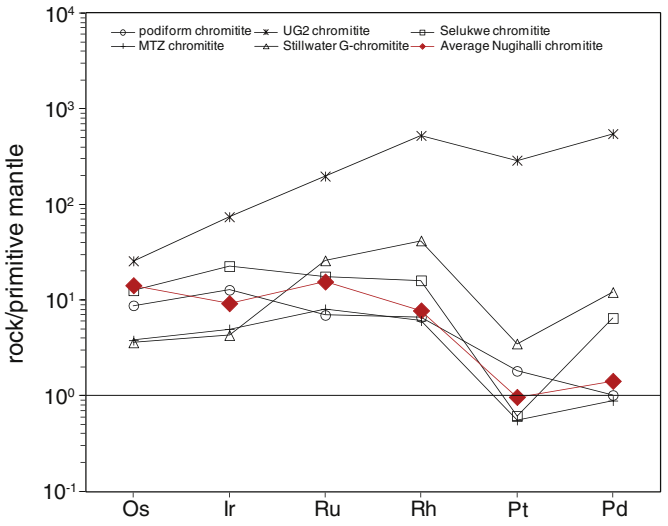

Fig. 11. Primitive mantle-normalized PGE patterns of average chromitites from our study compared with chromitites from layered intrusions (UG2 chromitite, Von Gruenewaldt and Merkle, 1995; Stillwater G-chromitite, Mondal and Zhou, 2010), ophiolites (podiform chromitite and Moho-Transition zone (MTZ) chromitite; Ahmed and Arai, 2002) and Archean greenstone belt (Selukwe greenstone belt, Zimbabwe craton; Mondal and Zhou, 2010).

pattern displayed by the gabbro and metavolcanic schists due to attainment of sulfide saturation.

Low-degree partial melts like MORB are sulfide-saturated (e.g., Hamlyn and Keays, 1986; Keays, 1995), such that they continue to segregate immiscible sulfides on slight fractionation of the silicate minerals when emplaced in crustal magma chambers. The continuously segregating immiscible sulfides, as well as the sulfides remnant in the mantle source of MORBs are responsible for concentrating platinum-group elements because of their chalcophile nature, thus making MORB unfit for hosting economic PGE deposits (e.g., Hamlyn and Keays, 1986). On the contrary, melts formed by high degrees of partial melting (≈20–25%) of an already depleted mantle are capable of extracting the remnant PGE-rich sulfides from the mantle source. Such 'second-stage' magmas are sulfide-undersaturated and when emplaced in the crust have the potential for forming economically important PGE deposits on attainment of sulfide-saturation. In these sulfide-undersaturated magmas, the PGEs behave as incompatible elements that are concentrated with progressive fractional crystallization in the residual magma, till the point when the magma attains sulfide saturation as an outcome of either fractionation of silicate minerals or by contamination of felsic crustal component or external crustal sulfur (e.g., Hamlyn and Keays, 1986 and references therein).

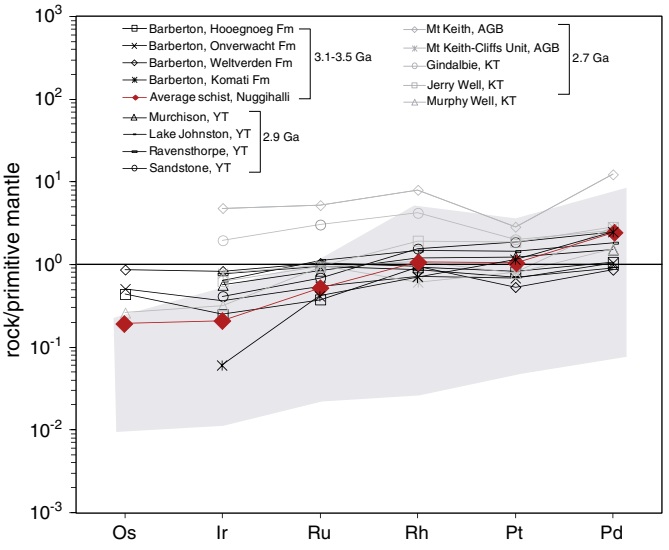

Fig. 12. Primitive mantle-normalized PGE patterns of average metavolcanic schists from our study normalized to 25 wt.% MgO and compared with early Archean and late Archean komatiites. Data of early Archean komatiites from 3.5 Ga Barberton greenstone belt (Kaapvaal craton, South Africa), and 2.9 Ga greenstone belts of Murchison, Lake Johnston, Sandstone and Ravensthorpe (Youanmi Terrane (YT), Western Australia). Late Archean komatiite data from the 2.7 Ga Mt. Keith Ultramafic Unit and Mt. Keith Cliffs unit (Agnew-Wiluna (AGB) greenstone belt, Western Australia), Murphy Well, John Terry (Gunbarrel flows) and Gindalbie (Acra) greenstone belts (Kurnalpi Terrane (KT), Western Australia). References are from Maier et al. (2009), Fiorentini et al. (2011) and references therein, and Barnes et al. (2012). Primitive-mantle values from McDonough and Sun (1995). The range of PGE abundances of metavolcanic schists from the Nuggihalli greenstone belt is shown by the gray field.

Sulfide saturation in magmas can be triggered by assimilation of siliceous crustal materials (Keays and Lightfoot, 2010) as sulfur solubility in basaltic magmas decreases on increasing the activity of silica (Buchanan, 1988). Crustal contamination is absent in the Nuggihalli rocks as is observed from the chondrite-normalized REE plots (Fig. 6), and the binary variation diagrams of La versus Sm, Th versus Yb, and Zr versus TiO_2 (Fig. 7). The absence of crustal contamination in komatiites and komatiitic basalts from the early Archean greenstone belts (≈3.4–3.1 Ga) of the Western Dharwar craton has also been supported by the work of Jayananda et al. (2008). Contamination of siliceous crustal materials is however not considered an efficient mechanism to trigger sulfide-saturation in komatiites, rather assimilation of sulfidic sediments is considered to be an important ore forming process (Fiorentini et al., 2010, 2012). There are reports of bedded barites from the stratigraphically equivalent Ghattihosahalli greenstone belt (Fig. 1a) in the Western Dharwar craton (Radhakrishna and Sreenivasaiah, 1974) which could prove to be a source of crustal sulfur, but none so far have been reported around the Nuggihalli greenstone belt. Presently it is difficult to constrain the role of crustal sulfur in bringing about sulfide saturation in the parental magma of the ultramafic–mafic rocks in the Nuggihalli greenstone belt. Sulfur isotope study may help us to identify the assimilation signature (e.g., Fiorentini et al., 2012) if any.

In the case of the Nuggihalli greenstone belt it appears that fractionation of olivine, pyroxene, and chromite from the Al-depleted komatiitic parental magma led to sulfide-saturation, which was induced by lowering of the activity of FeO in the melt (Buchanan, 1988). Sulfide disseminations are observed in magnetite, gabbro and a few metavolcanic schists in the greenstone belt, while the pyroxenite hosts inclusions of sulfides (2–15 μm) (Figs. 2 and 4d-e; Mukherjee et al., 2013). The immiscible sulfides segregated from the Al-depleted komatiitic parental magma, concentrating the PGE in them during crystallization of the pyroxenes that accumulated to form pyroxenite.

7. Conclusions

Despite low grade greenschist facies metamorphism and hydrothermal alteration of the ultramafic–mafic plutonic and metavolcanic (komatiitic to komatiitic basalt) schist rocks in the Nuggihalli greenstone belt, the majority of the trace elements (except La and Cu) and the PGEs behave in an immobile manner, based on their good correlation with MgO and Cr. The primitive-mantle normalized PGE patterns of the plutonic rocks are suggestive of fractionation of IPGEs by the early accumulated olivine and chromite minerals, and the incompatible nature of PPGEs during magma differentiation. The PPGE enriched trend in the metavolcanic schists indicates retention of IPGEs in the mantle source or IPGE-alloy saturation in the melt, while incompatible behavior of the PPGEs implies a sulfide-undersaturated nature of the mantle source. Chromitites have higher PGE abundance, especially IPGEs, due to the presence of inclusions of laurite and IPGE-bearing sulfarsenides. Primitive-mantle normalized metal patterns of chromitites show similarity with the IPGE-enriched pattern of sulfide-poor massive chromitites from ophiolites and layered intrusions, while the noble

metal patterns of the metavolcanic schists are comparable with those of the early Archean komatiites. The metavolcanic schists exhibit PGE depleted character typical of the early Archean komatiites which can be explained by progressive mixing of late veneer matter. Pt fractionation in the metavolcanic schists and in early and late Archean komatiites indicates dispersal of Pt-alloy in the lower mantle during crystallization of the primary magma ocean which formed isolated Pt-enriched and Pt-depleted upper mantle domains that did not homogenize by 2.7 Ga. Pyroxenite represents a break in the trend from sulfide-undersaturation to sulfide-saturation. Absence of geochemical signatures in our study for contamination of siliceous crustal materials along with the absence of ambient sulfidic sediments in the greenstone belt indicates that sulfide saturation in the parental magma of the Nuggihalli rocks was probably triggered by fractional crystallization of olivine, chromite and pyroxenes. The immiscible sulfides segregated from the Al-depleted komatiitic parental magma, concentrating the PGE during crystallization of the pyroxenes that accumulated to form pyroxenite.

Supplementary data to this article can be found online at http://dx.doi.org/10.1016/j.chemgeo.2014.08.007.

Acknowledgments

RM wishes to acknowledge the CSIR (New Delhi) for a fellowship to conduct this research as part of her PhD thesis project. RM acknowledges the support of M. Satyanarayanan and K.S.V. Subramanyam of the National Geophysical Research Institute (Hyderabad) for help during analytical work. M. Lingadevaru and K.S. Anantha Murthy are acknowledged for support during fieldwork. We are thankful to the late B.P. Radhakrishna and R.H. Sawkar for sharing views on the Nuggihalli greenstone belt. Igor Puchtel and Marco Fiorentini, the official reviewers of the journal are thankfully acknowledged for the critical review of this article. We are grateful to Laurie Reisberg, the Editor-in-Chief of the journal for her thoughtful and constructive comments that have helped to enhance the quality of the manuscript.

References

Ahmed, A.H., Arai, S., 2002. Unexpectedly high-PGE chromitite from the deeper mantle section of the northern Oman ophiolite and its tectonic implications. Contrib. Mineral. Petrol. 143, 263–278.

Alard, O., Griffin, W.L., Lorand, J.P., Jackson, S.E., O'Reilly, S.Y., 2000. Non-chondritic distribution of the highly siderophile elements in mantle sulphides. Nature 407, 891–894.

Arndt, N.T., Teixeira, N.A., White, W.M., 1989. Bizarre geochemistry of komatiites from the Crixas greenstone belt, Brazil. Contrib. Mineral. Petrol. 101, 187–197.

Arndt, N.T., Lesher, C.M., Barnes, S.J., 2008. Komatiite. Cambridge University Press, UK, (467 pp.).

Balaram, V., Ramavati, M., Banakar, V.K., Hein, J.R., Rao, C.R.M., Gnaneswara Rao, T., Dasaram, B., 2006. Determination of the platinum-group elements and gold in manganese nodule reference samples by nickel sulfide fire-assay and Te-coprecipitation with ICP-MS. Indian J. Mar. Sci. 35, 7–16.

Ballhaus, C., Bockrath, C., Wohlgemuth-Ueberwasser, C., Laurenz, V., Berndt, J., 2006. Fractionation of the noble metals by physical processes. Contrib. Mineral. Petrol. 152, 667–684.

Barnes, S.J., Fiorentini, M.L., 2008. Iridium, ruthenium and rhodium in komatiites: evidence for iridium alloy saturation. Chem. Geol. 257, 44–58.

Barnes, S.-J., Naldrett, A.J., Gorton, M.P., 1985. The origin of the fractionation of platinum-group elements in terrestrial magmas. Chem. Geol. 53, 303–323.

Barnes, S.-J., Boyd, R., Korneliussen, A., Nilsson, L.P., Often, M., Pedersen, R.B., Robins, B., 1988. The use of mantle normalization and metal ratios in discriminating between the effects of partial melting, crystal fractionation and sulphide segregation on platinum-group elements, gold, nickel, and copper: examples from Norway. In: Prichard, H.M., Potts, P.J., Bowles, S.J., Cripp, S.J. (Eds.), Proceedings of the Symposium Geoplatinum 87. Elsevier, London, pp. 113–143.

Barnes, S.J., Fiorentini, M.L., Fardon, M.C., 2012. Platinum group element and nickel sulphide ore tenors of the Mount Keith nickel deposit, Yilgarn Craton, Australia. Mineral. Deposita 47, 129–150.

Barnes, S.J., Heggie, G.J., Fiorentini, M.L., 2013. Spatial variation in platinum group element concentrations in ore-bearing komatiite at the Long-Victor deposit, Kambalda Dome, Western Australia: enlarging the footprint of nickel sulfide orebodies. Econ. Geol. 108, 913–933.

Borisov, A., Palme, H., 1997. Experimental determination of the solubility of platinum in silicate melts. Geochim. Cosmochim. Acta 61, 4349–4357.

Brenan, J.M., McDonough, W.F., Ash, R., 2005. An experimental study of the solubility and partitioning of iridium, osmium and gold between olivine and silicate melt. Earth Planet. Sci. Lett. 237, 855–872.

Brenan, J.M., Finnigan, C.F., McDonough, W.F., Homolova, V., 2012. Experimentalconstraints on the partitioning of Ru, Rh, Ir. Chem.Geol. 302–303, 16–32.

Brügmann, G.E., Arndt, N.T., Hofmann, A.W., Tobschall, H.J., 1987. Noble metalabundances in komatiite suites from Alexo, Ontario, and Gorgona-Island Colombia. Geochim. Cosmochim. Acta 51, 2159–2169.

Buchanan, D.L., 1988. Platinum-group element exploration. Developments in Economic Geology 26. Elsevier, Amsterdam, pp. 21–35.

Capobianco, C.J., Drake, M.J., 1990. Partitioning of ruthenium, rhodium, and palladium between spinel and silicate melt and implications for platinum group element fractionation trends. Geochim. Cosmochim. Acta 54, 869–874.

Chalapathi Rao, N.V., Lehmann, B., Balaram, V., 2014. Platinum-group element (PGE) geochemistry of Deccan orangeites, Bastar craton, central India: implication for a non-terrestrial origin for iridium enrichment at the K–Pg boundary. J. Asian Earth Sci. 84, 24–33.

Chou, C.-L., 1978. Fractionation of siderophile elements in the earth's upper mantle. Proceedings of the 9th Lunar and Planetary Science Conference. Geochimica et Cosmochimica Acta Supplement, pp. 219–230.

Devaraju, T.C., Alapieti, T.T., Kaukonen, R.J., Sudhakara, T.L., 2007. Petrological and PGE mineralization study of the Channagiri mafic-ultramafic complex, Shimoga supracrustal belt, Karnataka. J. Geol. Soc. India 70, 535–556.

Devaraju, T.C., Viljoen, R.P., Sawkar, R.H., Sudhakara, T.L., 2009. Mafic and ultramafic magmatism and associated mineralization in the Dharwar craton, southern India. J. Geol. Soc. India 73, 73–100.

DeWit, M.J., Tredoux, M., 1987. PGE in the 3.5 Ga Jamestown Ophiolite Complex, Barberton greenstone belt, with implications for PGE distribution in simatic lithosphere. In: Prichard, H.M., Potts, P.J., Bowles, J.F.W., Cribb, S.J. (Eds.), Proceedings of the Symposium GeoPlatinum, 87. Elsevier, London and New York, pp. 319–341.

Fiorentini, M.L., Beresford, S.W., Grguric, B., Barnes, S.J., Stone, W.E., 2007. Atypical stratiform sulfide-poor platinum-group element mineralization in the Agnew-Wiluna belt komatiites. J. Earth Sci. 54, 801–824.

Fiorentini, M.L., Barnes, S.J., Lesher, C.M., Heggie, G.J., Keays, R.R., Burnham, O.M., 2010. Platinum group element geochemistry of mineralized and nonmineralized komatiites and basalts. Econ. Geol. 105, 795–823.

Fiorentini, M.L., Barnes, S.J., Maier, W.D., Burnham, O.M., Heggie, G.J., 2011. Global variability in the platinum-group element contents of komatiites. J. Petrol. 52, 83–112.

Fiorentini, M.L., Beresford, S.W., Barley, M.E., Duuring, P., Bekker, A., Rosengren, N., Cas, R., Hronsky, J., 2012. District to camp controls on the genesis of komatiite-hosted nickel sulfide deposits, Agnew-Wiluna greenstone belt, Western Australia: insights from the multiple sulfur isotopes. Econ. Geol. 107, 781–796.

Ghiorso, M.S., Sack, R.O., 1995. Chemical mass transfer in magmatic processes. IV. A revised and internally consistent thermodynamic model for the interpolation and extrapolation of liquid–solid equilibria in magmatic systems at elevated temperatures and pressures. Contrib. Mineral. Petrol. 119, 197–212.

Hamlyn, P.R., Keays, R.R., 1986. Sulfur saturation and 2nd-stage melts–application to the Bushveld platinum metal deposits. Econ. Geol. 81, 1431–1445.

Hinchey, J.G., Hattori, K.H., Lavigne, M.J., 2005. Geology, petrology, and controls on PGE mineralization of the Southern Roby and Twilight Zones, Lac des Iles Mine, Canada. Econ. Geol. 100, 43–61.

Jafri, S.H., Khan, N., Ahmed, S.M., Saxena, R., 1983. Geology and Geochemistry of Nuggihalli Schist Belt, Dharwar Craton, Karnataka, India. In: Naqvi, S.M., Rogers, J.J.W. (Eds.), 4. Memoirs Geological Society of India, Precambrian of South India, pp. 110–120.

Jayananda, M., Kano, T., Peucat, J.J., Channabasappa, S., 2008. 3.35 Ga komatiite volcanism in the Western Dharwar craton, southern India: constraints from Nd isotopes and whole-rock geochemistry. Precambrian Res. 162, 160–179.

Keays, R.R., 1995. The role of komatiitic and picritic magmatism and S-saturation in the formation of ore deposits. Lithos 34, 1–18.

Keays, R.R., Lightfoot, P.C., 2010. Crustal sulfur is required to form magmatic Ni–Cu sulfide deposits: evidence from chalcophile element signatures of Siberian and Deccan Trap basalts. Mineral. Deposita 45, 241–257.

Keays, R.R., Ross, J.R., Woolrich, P., 1981. Precious metals in volcanic peridotite-associated nickel sulfide deposits in Western Australia. II: Distribution within the ores and the host rocks at Kambalda. Econ. Geol. 76, 1645–1674.

Leelananadam, C., Burke, K., Ashwal, L.D., Webb, S.J., 2006. Proterozoic mountain building in Peninsular India: an analysis based primarily on alkaline rock distribution. Geol. Mag. 143, 1–18.

Lesher, C.M., Keays, R.R., 2002. Komatiite-associated Ni–Cu-(PGE) deposits: mineralogy, geochemistry, and genesis. In: Cabri, L.J. (Ed.), The Geology, Geochemistry, Mineralogy, and Mineral Beneficiation of the Platinum-Group Elements 54. Canadian Institute of Mining, Metallurgy and Petroleum, pp. 579–617.

Locmelis, M., Pearson, N.J., Barnes, S.J., Fiorentini, M.L., 2011. Ruthenium in komatiitic chromite. Geochim. Cosmochim. Acta 75, 3645–3661.

Lorand, J.-P., Alard, O., 2001. Platinum-group element abundances in the upper mantle: new constraints from in-situ and whole-rock analyses of Massif Central xenoliths (France). Geochim. Cosmochim. Acta 65, 2789–2806.

Lorand, J.-P., Delpech, G., Grégoire, M., Moine, B., O'Reilly, S.Y., Cottin, J.-Y., 2004. Platinum-group elements and the multistage metasomatic history of Kerguelen lithospheric mantle (South Indian Ocean). Chem. Geol. 208, 195–215.

Lorand, J.P., Luguet, A., Alard, O., 2013. Platinum-group element systematics and petrogenetic processing of the continental upper mantle: a review. In: Mondal, S.K., Griffin, W.L., Maier, W.G. (Eds.), Ore Deposits and the Role of the Lithospheric Mantle 164–167. Lithos Special Issue, pp. 2–21.

Maier, W.D., Frederick, R., Barnes, S.-J., 2003. The concentration of the platinum-group elements in South African komatiites: implications for mantle sources, melting regime and PGE fractionation during crystallization. J. Petrol. 44, 1787–1804.
Maier, W.D., Barnes, S.J., Campbell, I.H., Fiorentini, M.L., Peltonen, P., Barnes, S.J., Smithies, R.H., 2009. Progressive mixing of meteoritic veneer into the early Earth's deep mantle. Nature 460, 620–623.
Mathez, E.A., 1999. On factors controlling the concentrations of platinum group elements in layered intrusions and chromitites. In: Keays, R.R., Lesher, C.M., Lightfoot, P.C., Farrow, C.E.G. (Eds.), Dynamic Processes in Magmatic Ore Deposits and Their Application in Mineral Exploration 13. Geological Association of Canada Short Course, pp. 251–285.
McDonough, W.F., Sun, S.-S., 1995. The composition of the Earth. Chem. Geol. 120, 223–253.
Mondal, S.K., Baidya, T.K., 1997. Platinum-group minerals from the Nuasahi ultramafic–mafic complex, Orissa, India. Mineral. Mag. 61, 902–906.
Mondal, S.K., Zhou, M.-F., 2010. Enrichment of PGE through interaction of evolved boninitic magmas with early formed cumulates in a gabbro–breccia zone of the Mesoarchean Nuasahi massif (eastern India). Mineral. Deposita 45, 69–91.
Mondal, S.K., Ripley, E.M., Li, C., Frei, R., 2006. The genesis of Archean chromitites from the Nuasahi and Sukinda massifs in the Singhbhum craton, India. Precambrian Res. 148, 45–66.
Moyen, J.-F., Martin, H., 2012. Forty years of TTG research. Lithos 148, 312–336.
Mukherjee, R., Mondal, S.K., Rosing, M.T., Frei, R., 2010. Compositional variations in the Mesoarchean chromites of the Nuggihalli schist belt, Western Dharwar craton (India): potential parental melts and implications for tectonic setting. Contrib. Mineral. Petrol. 160, 865–885.
Mukherjee, R., Mondal, S.K., Frei, R., Rosing, M.T., Waight, T.E., Zhong, H., Ravindra Kumar, G.R., 2012. The 3.1 Ga Nuggihalli chromite deposits, Western Dharwar craton (India): geochemical and isotopic constraints on mantle sources, crustal evolution and implications for supercontinent formation and ore mineralization. Lithos 155, 392–409.
Mukherjee, R., Mondal, S.K., González-Jiménez, J.M., Griffin, W.L., Pearson, N.J., O' Reilly, S. Y., 2013. Trace element fingerprints of chromites and sulfides from the Archean Nuggihalli greenstone belt, western Dharwar craton (India). Goldschmidt abstract. Mineral. Mag. 77, 1661–1817.
Murthy, N.G.K., 1987. Mafic dyke swarms of the Indian shield, Mafic swarms. Geol. Assoc. Can. 34, 393–400.
Naqvi, S.M., Ram Mohan, M., Rana Prathap, J.G., Srinivasa Sarma, D., 2009. Adakite–TTG connection and fate of Mesoarchaean basaltic crust of Holenarsipur Nucleus, Dharwar craton, India. J. Asian Earth Sci. 35, 416–434.
Nath, Swami, Ramakrishnan, M., 1981. Early Precambrian supracrustals of Karnataka. Mem.Geol.Surv. India 112, 26–28.
Nijagunappa, R., Naganna, C., 1983. Nuggihalli schist belt in the Karnataka craton: an Archaean layered complex as interpreted from chromite distribution. Econ. Geol. 79, 507–513.
Pandit, S.A., 1975. Mineragraphic study of titaniferous magnetite and associated sulfide minerals from Tagdur, Hassan district, Karnataka. Indian Minerals 14, 80–87.
Peach, C.L., Mathez, E.A., 1996. Constraints on the Formation of Platinum-Group Element Deposits in Igneous Rocks. Econ. Geol. 91, 439–450.
Peck, D.C., Scoates, R.F.J., Theyer, P., Desharnais, G., Hulbert, L.J., Huminicki, M.A.E., 2002. Stratiform and contact-type PGE-Cu-Ni mineralization in the Fox River Sill and the Bird River Belt, Manitoba. In: Cabri, L.J. (Ed.), The Geology, Geochemistry, Mineralogy and Mineral Beneficiation of Platinum-Group Elements 54. Canadian Institute of Mining and Metallurgy, pp. 367–387.
Prendergast, M.D., 2008. Archean komatiitic sill-hosted chromite deposits in the Zimbabwe Craton. Econ. Geol. 103, 981–1004.
Puchtel, I., Humayun, M., 2005. Highly siderophile element geochemistry of ^{187}Os-enriched 2.8-Ga Kostomuksha komatiites, Baltic Shield. Geochim. Cosmochim. Acta 69, 1607–1618.
Puchtel, I.S., Humayun, M., Campbell, A.J., Sproule, R.A., Lesher, C.M., 2004. Platinum group element geochemistry of komatiites from the Alexo and Pyke Hill areas, Ontario, Canada. Geochim. Cosmochim. Acta 68, 1361–1383.
Puchtel, I., Walker, R.J., Anhaeusser, C.R., Gruau, G., 2009. Re–Os isotope systematics and HSE abundances of the 3.5 Ga Schapenburg komatiites, South Africa: hydrous melting or prolonged survival of primordial heterogeneities in the mantle? Chem. Geol. 262, 355–369.
Puchtel, I.S., Walker, R., Touboul, M., Nisbet, E.G., Byerly, G.R., 2014. Insights into early Earth from the Pt-Re-Os isotope and highly siderophile element abundance systematics of Barberton komatiites. Geochim. Cosmochim. Acta 125, 394–413.
Qi, L., Zhou, M.F., Wang, C.Y., 2004. Determination of low concentrations of platinum group elements in geological samples by ID-ICP-MS. J. Anal. At. Spectrom. 19, 1335–1339.
Qi, L., Zhou, M.F., Wang, C.Y., Sun, M., 2007. Evaluation of the determination of Re and PGEs abundance of geological samples by ICP-MS coupled with a modified Carius tube digestion at different temperatures. Geochem. J. 41, 407–414.
Qi, L., Wang, C.Y., Zhou, M.F., 2008. Controls on the PGE distribution of Permian Emeishan alkaline and peralkaline volcanic rocks in Longzhoushan, Sichuan Province, SW China. Lithos 106, 222–236.
Radhakrishna, B.P., Naqvi, S.M., 1986. Precambrian continental crust of India and its evolution. J. Geol. 94, 145–166.
Radhakrishna, B.P., Sreenivasaiah, C., 1974. Bedded barites from the Precambrian of Karnataka. J. Geol. Soc. India 15, 314–315.
Radhakrishna, B.P., Vaidyanadhan, R., 1994. Geology of Karnataka. Geological Society of India, Bangalore, (298 pp.).
Radhakrishna, B.P., Pandit, S.A., Prabhakar, K.T., 1973. Copper mineralization in the Ultrabasic Complex of Nuggihalli, Hassan District, Mysore State. J. Geol. Soc. India 14, 302–312.
Ramakrishnan, M., 1981. Nuggihalli and Krishnarajpet belts. In: Swami Nath, J., Ramakrishnan, M. (Eds.), Early Precambrian supracrustals of southern Karnataka. Geological Survey of India Memoir No. 112, pp. 61–70.
Ramakrishnan, M., 2009. Precambrian mafic magmatism in the western Dharwar craton, Southern India. Geol. Soc. India 73, 101–116.
Rehkämper, M., Halliday, A.N., Fitton, J.G., Lee, D.-C., Wieneke, M., Arndt, N.T., 1999. Ir, Ru, Pt, and Pd in basalts and komatiites: new constraints for the geochemical behavior of the platinum-group elements in the mantle. Geochim. Cosmochim. Acta 63, 3915–3934.
Righter, K., Campbell, A.J., Humayun, M., Hervig, R.L., 2004. Partitioning of Ru, Rh, Pd, Re, Ir, and Au between Cr-bearing spinel, olivine, pyroxene and silicate melt. Geochim. Cosmochim. Acta 68, 867–880.
Rollinson, H., 1997. The Archaean komatiite-related Inyala chromitite, Southern Zimbabwe. Econ. Geol. 92, 98–107.
Roy, P., Balaram, V., Kumar, A., Satyanarayanan, M., Gnaneshwar Rao, T., 2007. New REE and trace element data on two Kimberlitic Reference materials by ICP-MS. Geostand. Geoana. Res. 31, 261–273.
Roy, P., Balaram, V., Sawant, S., Subramanyam, K.S.V., Satyanarayan, M., Vani, K., Srivalli, K., 2010. Determination of platinum group elements in kimberlites by ICP-MS: modified decomposition procedure using double NiS fire assay followed by Te co precipitation. At. Spectrosc. 31, 35–43.
Sattari, P., Brenan, J.M., Horn, I., McDonough, W.F., 2002. Experimental constraints on the sulfide-silicate and chromite-silicate melt partitioning behavior of rhenium and platinum-group elements. Econ. Geol. 97, 385–398.
Taylor, P.N., Chadwick, B., Friend, C.R.L., Ramakrishnan, M., Moorbath, S., Viswanatha, M.N., 1988. New age data on the geological evolution of Southern India. Workshop on the deep continental crust of South India, January 1988. J. Geol. Soc. India 31, 155–158.
Tredoux, M., Lindsey, N.M., Davies, G., McDonald, I., 1995. The fractionation of platinum group elements in magmatic systems, with the suggestion of a novel causal mechanism. S. Afr. J. Geol. 98, 157–167.
Von Gruenewaldt, G., Merkle, R.K.W., 1995. Platinum-group element proportions in chromitites of the Bushveld Complex: implications for fractionation and magma mixing models. J. Afr. Earth Sci. 21, 615–632.
Whitney, D.L., Evans, B.W., 2010. Abbreviations for names of rock-forming minerals. Am. Mineral. 95, 185–187.
Zhou, M.-F., 1994. PGE distribution in 2.7 Ga layered komatiite flows from the Belingwe greenstone belt, Zimbabwe. Chem. Geol. 118, 155–172.
Zhou, M.-F., Sun, M., Keays, R.R., Kerrich, R.W., 1998. Controls on platinum-group elemental distributions of podiform chromitites: a case study of high-Cr and high-Al chromitites from Chinese orogenic belts. Geochim. Cosmochim. Acta 62, 677–688.